

## TRACTABLE OPTIMAL EXPERIMENTAL DESIGN USING TRANSPORT MAPS

KARINA KOVAL, ROLAND HERZOG, AND ROBERT SCHEICHL

ABSTRACT. We present a flexible method for computing Bayesian optimal experimental designs (BOEDs) for inverse problems with intractable posteriors. The approach is applicable to a wide range of BOED problems and can accommodate various optimality criteria, prior distributions and noise models. The key to our approach is the construction of a transport-map-based surrogate to the joint probability law of the design, observational and inference random variables. This order-preserving transport map is constructed using tensor trains and can be used to efficiently sample from (and evaluate approximate densities of) conditional distributions that are used to define many commonly-used optimality criteria. The algorithm is also extended to sequential data acquisition problems, where experiments can be performed in sequence and used to update the state of knowledge about the unknown parameters. The sequential BOED problem is made computationally feasible by preconditioning the approximation of the joint density at the current stage using transport maps constructed at previous stages. The flexibility of our approach in finding optimal designs is illustrated with some numerical examples inspired by disease modeling and the reconstruction of subsurface structures in aquifers.

## 1. INTRODUCTION

The Bayesian approach to parameter estimation is widespread throughout the sciences and engineering. In the Bayesian framework, a-priori knowledge (encoded in a prior measure) of some unknown/unobservable parameters is updated using experimental data and a mathematical model. Hence, the solution to the Bayesian inverse problem is a posterior probability law describing the updated state of knowledge conditioned on the observed data. The quality of the solution is highly dependent on the observed experimental data — a poorly-chosen experimental setup can lead to uninformed posteriors not straying far from the prior, whereas well-chosen experimental designs can lead to well-informed posteriors characterized by high degrees of certainty.

In many Bayesian inverse problems stemming from real-world phenomena, there are limitations on the number of experiments that can be performed or the amount of data that can be acquired. These limitations could originate from physical or monetary constraints. For example, tsunami warning systems rely on pressure sensors tethered to the ocean floor near trenches, and groundwater monitoring systems require drilling wells deep into the ground — both scenarios are characterized by expensive means of data acquisition. In such settings, it is crucial to allocate the limited resources well, choosing experimental conditions that maximize the “quality” of the measured data.

Optimal experimental design (OED) provides a rigorous mathematical framework for addressing the question of how to design experimental conditions for optimal parameter inference. Standard OED references in the point estimation setting include [43, 48, 44, 8], and the techniques found therein have gained much traction within the last few decades in the Bayesian inverse problems community. In OED, experimental designs are chosen to optimize some utility function that assesses the amount of information that could be gleaned from performing any feasible experiment. The utility functions are user-specified and problem-dependent, though there is a plethora of commonly used criteria. For any design, these commonly used criteria (e. g., A-, D-, E-optimality [1]) evaluate the statistical quality of

---

2010 *Mathematics Subject Classification.* 62K05, 62F15, 65K10, 65L09, 65N21, 15A69.

*Key words and phrases.* optimal experimental design, Bayesian inverse problems, uncertainty quantification, transportation of measures, low-rank tensor decomposition, tensor trains.

This work has been partially funded by Carl Zeiss-Stiftung through the project “Model-Based AI: Physical Models and Deep Learning for Imaging and Cancer Treatment”. RS and KK would like to thank the Isaac Newton Institute for Mathematical Sciences for support and hospitality during the programme on *Future Data-Driven Engineering* when part of the work on this paper was undertaken, supported by EPSRC grant number EP/R014604/1.

the resulting posterior distribution. The overarching goal is to choose designs or experimental conditions that minimize the level of uncertainty, or maximize information, in the posterior.

Solving the OED optimization problem is challenging for Bayesian inverse problems governed by models that involve systems of ordinary differential equations (ODEs) or even partial differential equations (PDEs). Since the Bayesian inverse problem is merely a sub-problem of OED, all the numerical challenges present in Bayesian inference due to, e.g., the large number of inference parameters and the expensive-to-evaluate PDE/ODE models, are inherited. Many efficient and scalable algorithms for solving these challenging high-dimensional (or infinite-dimensional) OED problems have been developed in recent years [33, 4, 32, 2, 5, 39, 26, 1, 6, 25, 3, 10, 11, 50]. A large portion of these techniques (see, e.g., [29, 4, 7, 9, 39, 34, 6, 10]) are formulated for *linear* Bayesian inverse problems with additive Gaussian noise models and Gaussian priors. For such problems, the parameter enters linearly into the parameter-to-observable (PTO) map and the posteriors are Gaussian, hence simple to characterize.

In this article, we focus on the design of experimental conditions for Bayesian inverse problems governed by *nonlinear* PTO maps, or with non-Gaussian priors, resulting in Bayesian inverse problems characterized by non-Gaussian posteriors. The nonlinear parameter-to-observable map introduces some unique challenges that are not present in the linear OED setting, even under the assumption of an additive Gaussian noise model — the most notable of which are lack of a closed-form expression for the utility function, and the dependence of the optimality criterion on the observed data. The latter issue is often circumvented by finding designs that work well on average for all realizations of the data, i.e., by optimizing the expected value of the chosen utility function. However, even after this simplification, the former challenge of approximating the resulting objective function remains. A few common approaches for alleviating this challenge involve: linearization techniques (e.g., using a Laplace approximation to the posterior as in [37, 5]) or purely sample-based nested Monte Carlo techniques, made computationally feasible via a surrogate approximation to the parameter-to-observable map [33, 50].

**Our approach.** The approach presented in this paper follows the latter set of techniques. That is, sticking with the non-Gaussian posterior, in Section 3 we focus our attention on designing computationally tractable sample-based approximations to the expected utility function. This is achieved by building a transport map that pushes forward a tractable reference density (e.g., multivariate Gaussian) to the intractable *joint* density for the design, observation and inference random variables. This transport map can be used to obtain independent and identically distributed (i.i.d.) samples for Monte Carlo approximation to the expected utility for any feasible design for various choices of the utility function.

Transport maps have been used for modeling and exploring posterior distributions in Bayesian inverse problems (see, e.g., [38, 42, 14, 15]), and have also made an appearance in the OED literature (see, e.g., [31, 12]). In [12], sample-based transport maps are used to approximate the information contained in various summary statistics of image data, with the ultimate goal of reducing data volume. In contrast, our focus is choosing experimental conditions that maximize information content of sparse data. Since the data distribution in our applications depends on the design, we learn the joint density for the data, inference parameter, and design random variables. This enables approximation of the expected utility function for various designs using a single transport map. In [31], a transport map to the joint density on the designs, observations and inference parameters is also constructed, but our approach differs in the following key ways: (i) we employ a functional tensor train (FTT) based transport map following [20] and thus take a function approximation viewpoint rather than a sample-based density approximation approach; (ii) we target a wide class of Bayesian experimental design problems and optimality criteria, whereas the aforementioned work deals primarily with finding sequential optimal designs (SOEDs) maximizing expected information gain.

**Contributions.** The main contributions of the work presented here are as follows: (i) We formulate a computationally tractable transport map approach for approximating expected utility functions appearing in Bayesian OED problems. The approach presented is applicable to a wide range of optimality criteria, design types, and prior models, and is thus highly flexible. (ii) We extend the base methodology for finding sequentially optimal designs in a greedy fashion. To make the sequential OED procedure

computationally feasible, we propose recycling previously learned information into suitably chosen preconditioners to speed up subsequent computations. (iii) We present a numerical study that illustrates the effectiveness and flexibility of the proposed approach for two types of design problems.

**Limitations and Outlook.** Of course, the approach is not without limitations, which include: (i) While the approach works well in practice for problems with a *moderate* number of inference parameters, the presented algorithms are typically infeasible for very high- or infinite-dimensional problems. This can be circumvented with a-priori dimensionality reduction using, e. g., an extension of the reparametrization techniques presented in [20, Section 3]. (ii) Likewise, the approach works well for finding optimal designs for a small to moderate number of experiments, i. e., in the small data regime, which is the primary focus in this article. (iii) It is clear from the design comparisons presented in Section 5 that the approach seems to work well in practice, however, a theoretical study of the approximation error and rank bounds for the FTT-based transport map surrogates will be crucial to garner a better understanding of the suitability and limitations of our approach. First steps to obtain such theoretical guarantees for Gaussian densities can be found in [45].

**Outline.** In Section 2 we outline relevant prerequisite material on the Bayesian approach to inverse problems, Bayesian optimal experimental design, and the conditional sampling framework introduced in [20]. In Section 3 we present our transport map-based approach for Bayesian batch OED, which builds on the ideas proposed in the aforementioned paper. Section 4 extends our method for guiding data acquisition in a sequential fashion, i. e., for adaptive OED. In Section 5, we illustrate our method with two numerical examples.

## 2. BACKGROUND

In this section, we present notation and some relevant preliminary material. Additionally, we summarize some key concepts from [24, 19, 20] that lay the foundation for our method.

**2.1. Bayesian Inverse Problems.** We consider the inverse problem of inferring an unknown / unobservable vector of parameters  $\mathbf{m} \in \mathcal{M}$  from observations of a quantity  $\mathbf{d} \in \mathcal{D}$ , related to  $\mathbf{m} = [m_1, m_2, \dots, m_{n_m}]^T$  through the model:

$$(2.1) \quad \mathbf{d} = \mathcal{F}(\mathbf{m}) + \boldsymbol{\eta},$$

where  $\mathcal{F}: \mathcal{M} \rightarrow \mathcal{D}$  denotes the parameter-to-observable (PTO) map and  $\boldsymbol{\eta} \in \mathbb{R}^{n_d}$  refers to the measurement noise. The problem-dependent parameter space  $\mathcal{M} \subseteq \mathbb{R}^{n_m}$  and observation space  $\mathcal{D} \subseteq \mathbb{R}^{n_d}$  are assumed to be finite-dimensional. Additionally, we make the common assumption of an additive Gaussian noise model, though our method could be extended to incorporate other noise models. In many typical applications,  $\mathcal{F} := \mathcal{O} \circ \mathcal{G}$  is defined as the composition of a parameter-to-state map  $\mathcal{G}: \mathbb{R}^{n_m} \rightarrow \mathcal{U}$ , where  $\mathcal{U}$  can denote a finite-dimensional or infinite-dimensional vector space, and an observation operator  $\mathcal{O}: \mathcal{U} \rightarrow \mathbb{R}^{n_d}$ . The observation operator maps the state  $u \in \mathcal{U}$  to the observable quantity  $\mathbf{d} = [d_1, d_2, \dots, d_{n_d}]^T$ . For example, in the simplest case,  $\mathcal{O}$  can denote a (smoothed) point evaluation operator. Of particular interest in this work are inverse problems where the parameter-to-state operator is expensive to apply, e. g., the parameter-to-state or *forward map* could be defined implicitly through the solution of a PDE or a system of ODEs. In this case, the parameter vector  $\mathbf{m}$  typically parametrizes some functional input to the forward operator.

The Bayesian approach is a probabilistic approach to solving inverse problems. Given a prior probability measure on  $\mathbf{m}$ , denoted by  $\mu_{\mathbf{m}}$  with corresponding Lebesgue density  $\pi_{\mathbf{m}}$ , and mean-zero additive Gaussian noise,  $\boldsymbol{\eta} \sim \mathcal{N}(\mathbf{0}, \Gamma_{\boldsymbol{\eta}})$ , the solution to the Bayesian inverse problem is a posterior probability law. In the finite-dimensional parameter inference setting, the posterior law has a corresponding posterior density that can be obtained using Bayes' law,

$$(2.2) \quad \pi_{\mathbf{m}|\mathbf{d}}(\mathbf{m} | \mathbf{d}) = \frac{\pi_{\mathbf{d}|\mathbf{m}}(\mathbf{d} | \mathbf{m}) \pi_{\mathbf{m}}(\mathbf{m})}{\pi_{\mathbf{d}}(\mathbf{d})}.$$

The conditional density  $\pi_{\mathbf{d}|\mathbf{m}}$ , the so-called likelihood, satisfies  $\pi_{\mathbf{d}|\mathbf{m}}(\mathbf{d} | \mathbf{m}) \propto \exp(-\frac{1}{2}\|\mathcal{F}(\mathbf{m}) - \mathbf{d}\|_{\mathbf{\Gamma}_\eta^{-1}}^2)$  due to the assumption of additive Gaussian measurement noise. Throughout, for any symmetric positive-definite matrix  $\mathbf{W} \in \mathbb{R}^{n \times n}$  we use  $\|\cdot\|_{\mathbf{W}}$  to denote the  $\mathbf{W}$ -weighted norm, i. e., for any  $\mathbf{x} \in \mathbb{R}^n$ ,  $\|\mathbf{x}\|_{\mathbf{W}}^2 := \mathbf{x}^T \mathbf{W} \mathbf{x}$ . The so-called evidence  $\pi_{\mathbf{d}}$  is typically unknown.

We note that for Bayesian inverse problems where the parameter  $\mathbf{m}$  enters nonlinearly into  $\mathcal{F}$ , the posterior  $\pi_{\mathbf{m}|\mathbf{d}}$  is typically non-Gaussian (even with the assumption of Gaussian prior and additive Gaussian noise) and often there is no closed-form expression for the density. This is also the case if the prior is non-Gaussian, even with a linear PTO. In such cases, one can only probe the posterior distribution, e. g., by computing various moments or statistics like the maximum a-posteriori estimator (commonly referred to as the MAP point) using sampling techniques such as Markov chain Monte Carlo (MCMC) [30].

**2.2. Optimal Experimental Design for Bayesian Inverse Problems with Non-Gaussian Posteriors.** The quality of the solution to the Bayesian inverse problem depends crucially on the quality and quantity of the measured data. Guiding data acquisition or choosing experimental conditions for “optimal” inference of the unknown parameters  $\mathbf{m}$  requires solving an optimal experimental design problem. The definition of “experimental design” is typically problem-specific. For example, in sensor placement problems, the design could correspond to the spatial coordinates at which the state  $u$  is observed. Alternatively, the design could enter the parameter-to-state map  $\mathcal{G}$  *intrusively* as a boundary/initial condition.

In the following, we assume that the design can be expressed using the variable  $\mathbf{e} \in \mathcal{E} \subset \mathbb{R}^{n_e}$  and enters into the model through the parameter-to-observable map ( $\mathcal{F}: \mathcal{E} \times \mathcal{M} \rightarrow \mathcal{D}$ ) as well as the noise model ( $\boldsymbol{\eta} \sim \mathcal{N}(\mathbf{0}, \mathbf{\Gamma}_\eta(\mathbf{e}))$ ). The design dependence of the model and thus of the likelihood  $\pi_{\mathbf{d}|\mathbf{e},\mathbf{m}}(\mathbf{d} | \mathbf{e}, \mathbf{m}) \propto \exp(-\frac{1}{2}\|\mathcal{F}(\mathbf{e}, \mathbf{m}) - \mathbf{d}\|_{\mathbf{\Gamma}_\eta(\mathbf{e})^{-1}}^2)$  leads to a design-dependent posterior distribution with density

$$(2.3) \quad \pi_{\mathbf{m}|\mathbf{e},\mathbf{d}}(\mathbf{m} | \mathbf{e}, \mathbf{d}) = \frac{\pi_{\mathbf{d}|\mathbf{e},\mathbf{m}}(\mathbf{d} | \mathbf{e}, \mathbf{m}) \pi_{\mathbf{m}}(\mathbf{m})}{\pi_{\mathbf{d}|\mathbf{e}}(\mathbf{d} | \mathbf{e})}.$$

Note that (2.3) is obtained by employing the common assumption that the prior density is independent of the design, i. e.,  $\pi_{\mathbf{m}|\mathbf{e}} \equiv \pi_{\mathbf{m}}$ .

Similar to the definition of design, what defines an “optimal” design is also problem-specific. For Bayesian inverse problems with non-Gaussian posteriors, optimal designs are often chosen to optimize some expected utility function, i. e.,

$$(2.4) \quad \mathbf{e}^* \in \underset{\mathbf{e} \in \mathcal{E}}{\text{Arg max}} \mathbb{E}_{\pi_{\mathbf{d}|\mathbf{e}}}[\psi(\mathbf{e}, \mathbf{d})].$$

For any design  $\mathbf{e} \in \mathcal{E}$  and corresponding measured data  $\mathbf{d} \in \mathcal{D}$ , the utility function  $\psi(\mathbf{e}, \mathbf{d})$  evaluates the quality of the solution to the resulting Bayesian inverse problem. This risk-neutral formulation chooses designs that maximize the user-specified utility function on average for all possible realizations of the data. While there are many options for the utility function leading to different optimal designs, for illustrative purposes we focus on two commonly used criteria in the Bayesian OED literature, A- and D-optimality.

The *A-optimality* criterion seeks designs that minimize the expected value of the average posterior variance in the inference parameters. This is equivalent to maximizing the expected value of the A-optimal utility function  $\psi_A$ , defined as

$$(2.5) \quad \psi_A(\mathbf{e}, \mathbf{d}) := -\text{trace}[\mathbf{C}_{\mathbf{m}|\mathbf{e},\mathbf{d}}(\mathbf{e}, \mathbf{d})].$$

Here  $\mathbf{C}_{\mathbf{m}|\mathbf{e},\mathbf{d}}(\mathbf{e}, \mathbf{d}) = \mathbb{E}_{\pi_{\mathbf{m}|\mathbf{e},\mathbf{d}}}[(\mathbf{m} - \mathbf{m}_{\text{post}}^{\mathbf{e},\mathbf{d}})(\mathbf{m} - \mathbf{m}_{\text{post}}^{\mathbf{e},\mathbf{d}})^T]$  denotes the posterior covariance matrix with posterior mean  $\mathbf{m}_{\text{post}}^{\mathbf{e},\mathbf{d}} := \mathbb{E}_{\pi_{\mathbf{m}|\mathbf{e},\mathbf{d}}}[\mathbf{m}]$ .

On the other hand, taking an information-theoretic viewpoint, the Bayesian *D-optimal* design maximizes the *expected information gain* (EIG) from prior to posterior (see, e. g., [36]). Thus the D-optimal utility function  $\psi_D$  is defined as the Kullback-Leibler (KL) divergence of the posterior from the prior,

$$(2.6) \quad \psi_D(\mathbf{e}, \mathbf{d}) := \mathcal{D}_{\text{KL}}(\pi_{\mathbf{m}|\mathbf{e},\mathbf{d}} \| \pi_{\mathbf{m}}) = \mathbb{E}_{\pi_{\mathbf{m}|\mathbf{e},\mathbf{d}}} \left[ \log \left( \frac{\pi_{\mathbf{m}|\mathbf{e},\mathbf{d}}}{\pi_{\mathbf{m}}} \right) \right].$$

We emphasize that for non-Gaussian posteriors, there are typically no closed-form expressions for the utility functions  $\psi_A$  and  $\psi_D$ . Thus, it is a significant challenge to evaluate these criteria and their expected values, denoted respectively by  $\Psi_A$  and  $\Psi_D$ . To address the latter, we take a sample average approximation (SAA) approach, which leads to the discretized A- and D-optimality criteria:

$$(2.7) \quad \Psi_A(\mathbf{e}) \approx -\frac{1}{N} \sum_{i=1}^N \text{trace}[\mathbf{C}_{\mathbf{m}|\mathbf{e}, \mathbf{d}^{(i)}}(\mathbf{e}, \mathbf{d}^{(i)})] =: \widehat{\Psi}_A^N(\mathbf{e})$$

$$(2.8) \quad \Psi_D(\mathbf{e}) = \mathbb{E}_{\pi_{\mathbf{d}, \mathbf{m}|\mathbf{e}}} \left[ \log \left( \frac{\pi_{\mathbf{m}|\mathbf{e}, \mathbf{d}}}{\pi_{\mathbf{m}}} \right) \right] \approx \frac{1}{N} \sum_{i=1}^N \log \left( \frac{\pi_{\mathbf{m}|\mathbf{e}, \mathbf{d}^{(i)}}(\mathbf{m}^{(i)})}{\pi_{\mathbf{m}}(\mathbf{m}^{(i)})} \right) =: \widehat{\Psi}_D^N(\mathbf{e}).$$

The first equality in (2.8) is obtained via another application of Bayes' law.

However, the aforementioned challenge of evaluating the summands remains. Exact evaluation of each summand is generally infeasible, and some efficient approximation is needed. These approximations typically require access to the posterior distribution for many realizations of the data and design. Additionally, in defining both criteria, we have assumed the ability to sample from generally intractable distributions, i. e.,  $\mathbf{d}^{(i)} \sim \pi_{\mathbf{d}|\mathbf{e}}$  in (2.7) and  $(\mathbf{d}^{(i)}, \mathbf{m}^{(i)}) \sim \pi_{\mathbf{d}, \mathbf{m}|\mathbf{e}}$  in (2.8) for any design choice  $\mathbf{e} \in \mathcal{E}$ . While efficient MCMC methods for obtaining these samples and thus exploring intractable distributions have been developed in recent years (see, e. g., [23, 22]), using these approaches to solve the OED problem would require generating a different set of samples for each design realization in an iterative optimization algorithm, which can get prohibitively expensive.

An alternative approach that enables rapid sampling from the joint density  $\pi_{\mathbf{d}, \mathbf{m}}$  as well as from the marginal  $\pi_{\mathbf{d}}$  and conditional  $\pi_{\mathbf{m}|\mathbf{d}}$  for any fixed design is based on transportation of measure. The idea is to construct a deterministic coupling between a product-form reference distribution  $\nu_{\mathbf{d}, \mathbf{m}}$  and the joint distribution for the observational and inference random variables  $\mu_{\mathbf{d}, \mathbf{m}}$ . A particular choice of this coupling, or transport map, called the Knothe-Rosenblatt rearrangement, offers a way to obtain i. i. d. samples from the posterior distribution and an explicit representation of the posterior density  $\pi_{\mathbf{m}|\mathbf{d}}$  for any  $\mathbf{d} \in \mathcal{D}$ . In the following section, we summarize the key tools and ideas of the approach presented in [20] that we extend to OED in Section 3.

### 2.3. Conditional Sampling Using Inverse Knothe-Rosenblatt Transports and Tensor Trains.

In [20], the authors propose an offline-online approach to Bayesian parameter inference. The majority of the computational resources are expended in an offline phase, where a transport map surrogate is built that then enables rapid online approximation of posterior statistics for any realization of the data. A crucial tool for realizing their approach is the *Knothe-Rosenblatt* (KR) rearrangement ([46, 49]).

Given a target random variable  $\mathbf{x} = [x_1, \dots, x_n]^T \in \mathcal{X} \subset \mathbb{R}^n$  and a reference random variable  $\mathbf{v} = [v_1, \dots, v_n]^T \in \mathcal{V} \subset \mathbb{R}^n$  with probability laws  $\mu_{\mathbf{x}}$  and  $\nu_{\mathbf{v}}$ , respectively, the *KR rearrangement* defines a triangular, order-preserving diffeomorphism  $\mathcal{T}: \mathcal{V} \rightarrow \mathcal{X}$  that couples the random variables  $\mathbf{x}$  and  $\mathbf{v}$ . The general structure of  $\mathcal{T}$  is

$$(2.9) \quad \mathcal{T}(\mathbf{v}) = \begin{bmatrix} x_1 \\ x_2 \\ \vdots \\ x_n \end{bmatrix} = \begin{bmatrix} \mathcal{T}_{x_1}(v_1) \\ \mathcal{T}_{x_2|x_1}(\mathbf{v}_{1:2}) \\ \vdots \\ \mathcal{T}_{x_n|x_{1:n-1}}(\mathbf{v}) \end{bmatrix},$$

where the notation  $\mathbf{x}_{1:k} = (x_1, x_2, \dots, x_k)$  is used to denote the first  $k$  components of  $\mathbf{x}$ . Note that by *order-preserving*, we mean that each component  $\mathcal{T}_{x_k|x_{1:k-1}}: \mathbb{R}^k \rightarrow \mathbb{R}$  is strictly monotonically increasing in the last variable,  $v_k$ . Under this map, the pushforward of  $\nu_{\mathbf{v}}$  is the law of the image  $\mathcal{T}(\mathbf{v})$  and is denoted by  $\mathcal{T}_\# \nu_{\mathbf{v}}$ , and the pullback of  $\mu_{\mathbf{x}}$  is the law of the random variable  $\mathcal{T}^{-1}(\mathbf{x})$  denoted by  $\mathcal{T}^\# \mu_{\mathbf{x}}$ . We only consider measures that are absolutely continuous with respect to the Lebesgue measure, such that the pushforward and pullback operators define transformations between the target density  $\pi_{\mathbf{x}}$  (corresponding

to  $\mu_{\mathbf{x}}$ ) and the reference density  $\rho_{\mathbf{v}}$  (corresponding to  $\nu_{\mathbf{v}}$ ) via the change-of-variables formulae

$$\begin{aligned}\pi_{\mathbf{x}}(\mathbf{x}) &= \mathcal{T}_{\sharp}^{\dagger} \rho_{\mathbf{v}}(\mathbf{x}) = \rho_{\mathbf{v}}(\mathcal{T}^{-1}(\mathbf{x})) \det(D\mathcal{T}^{-1}(\mathbf{x})), \\ \rho_{\mathbf{v}}(\mathbf{v}) &= \mathcal{T}^{\sharp} \pi_{\mathbf{x}}(\mathbf{v}) = \pi_{\mathbf{x}}(\mathcal{T}(\mathbf{v})) \det(D\mathcal{T}(\mathbf{v})),\end{aligned}$$

where  $D$  denotes the Jacobian of the respective map.

In the offline phase of the approach presented in [20], the KR rearrangement is employed to build a coupling between a product-form reference density  $\rho_{\mathbf{d},\mathbf{m}}(\mathbf{v}_d, \mathbf{v}_m) = \rho_{\mathbf{d}}(\mathbf{v}_d) \rho_{\mathbf{m}}(\mathbf{v}_m)$  and the joint density on the observation and inference parameter random variables  $\pi_{\mathbf{d},\mathbf{m}}(\mathbf{d}, \mathbf{m}) = \pi_{\mathbf{d}|\mathbf{m}}(\mathbf{d}|\mathbf{m}) \pi_{\mathbf{m}}(\mathbf{m})$ . Partitioning the target random variables as  $\mathbf{x} = (\mathbf{d}, \mathbf{m})$  and the reference random variables as  $\mathbf{v} = (\mathbf{v}_d, \mathbf{v}_m)$ , the KR rearrangement (2.9) can be written in block form,

$$(2.10) \quad \mathcal{T}(\mathbf{v}_d, \mathbf{v}_m) = \begin{bmatrix} \mathbf{d} \\ \mathbf{m} \end{bmatrix} = \begin{bmatrix} \mathcal{T}_d(\mathbf{v}_d) \\ \mathcal{T}_{\mathbf{m}|\mathbf{d}}(\mathbf{v}_d, \mathbf{v}_m) \end{bmatrix}.$$

Not only does the KR rearrangement offer computational benefits due to its triangular structure, the map also “exposes” conditional densities. This latter property is what makes the KR map well-suited for posterior sampling. For any  $\mathbf{d}^* \in \mathcal{D}$ , if  $\mathbf{v}_m \sim \rho_{\mathbf{m}}$ , then the random variable defined using the map  $\mathcal{T}_{\mathbf{m}|\mathbf{d}}(\mathcal{T}_d^{-1}(\mathbf{d}^*), \mathbf{v}_m)$  follows the posterior density  $\pi_{\mathbf{m}|\mathbf{d}^*} := \pi_{\mathbf{m}|\mathbf{d}=\mathbf{d}^*}$ . This conditional transport map enables rapid online sample generation and density evaluation from the posterior distribution for any data instance.

Construction of the true map  $\mathcal{T}$  is in general not feasible and various approximation techniques have been developed (see, e.g., [47, 35, 13, 14, 41, 21]). Many approaches define the map *implicitly* as the minimizer of a sample-based approximation to the KL divergence between the target density and its approximation over some parametrized class of triangular transport maps. In contrast, in [20], an *explicit* transport map is constructed to couple the reference density to a tensor train (TT) *approximation* to the joint density. For completeness we summarize the procedure and main ideas, but refer to the aforementioned paper for technical details.

To start, a tensor train surrogate is built to approximate the square root of the multivariate joint density  $(\pi_{\mathbf{d},\mathbf{m}})$  as the product of matrix-valued univariate functions,

$$(2.11) \quad \sqrt{\pi_{\mathbf{d},\mathbf{m}}(\mathbf{d}, \mathbf{m})} \approx g_{\mathbf{d},\mathbf{m}}(\mathbf{d}, \mathbf{m}) = \prod_{i=1}^{n_d+n_m} \tilde{\mathbf{G}}_i(x_i) := \prod_{i=1}^{n_d} \mathbf{G}_i^d(d_i) \prod_{j=1}^{n_m} \mathbf{G}_j^m(m_j).$$

In general, a rank-truncated TT approximation does not preserve non-negativity properties of the target function. Constructing the TT surrogate to the square root of the target density circumvents this challenge and ensures the resulting approximation is non-negative. The functions  $\tilde{\mathbf{G}}_i: \mathbb{R} \rightarrow \mathbb{R}^{r_{i-1} \times r_i}$  are referred to as the TT cores and have dimensions defined by the ranks  $r_i$  with  $r_0 = r_{n_d+n_m} = 1$ . Such a decomposition can be built with

$$(2.12) \quad \mathcal{O}\left(\sum_{i=1}^{n_d+n_m} r_{i-1} r_i\right)$$

evaluations of the (*unnormalized*) joint density  $\pi_{\mathbf{d},\mathbf{m}}$  using efficient alternating-direction cross approximation methods; for details see [40, 24] and [20, Appendix B.1]. Once  $g_{\mathbf{d},\mathbf{m}}$  is computed, a non-negative approximation (denoted by  $p_{\mathbf{d},\mathbf{m}}$ ) to the normalized density  $\pi_{\mathbf{d},\mathbf{m}}$  can be obtained,

$$(2.13) \quad \pi_{\mathbf{d},\mathbf{m}}(\mathbf{d}, \mathbf{m}) \approx p_{\mathbf{d},\mathbf{m}}(\mathbf{d}, \mathbf{m}) \propto g_{\mathbf{d},\mathbf{m}}(\mathbf{d}, \mathbf{m})^2.$$

We note that tuning the parameters in the construction algorithm, e.g., the dimensions of the matrices  $\tilde{\mathbf{G}}_i$ , provides some control over the approximation error measured using f-divergences. For example, the dimensions could be chosen to ensure that the Hellinger distance

$$\begin{aligned}\mathcal{D}_{\text{H}}(p_{\mathbf{d},\mathbf{m}}, \pi_{\mathbf{d},\mathbf{m}}) &= \left(\frac{1}{2} \int (\sqrt{p_{\mathbf{d},\mathbf{m}}} - \sqrt{\pi_{\mathbf{d},\mathbf{m}}})^2 \, d\mathbf{d} \, d\mathbf{m}\right)^{\frac{1}{2}} \\ &= \frac{1}{\sqrt{2}} \|\sqrt{p_{\mathbf{d},\mathbf{m}}} - \sqrt{\pi_{\mathbf{d},\mathbf{m}}}\|_{L_2}\end{aligned}$$

is bounded from above by some tolerance  $\varepsilon$ , i. e.,  $\mathcal{D}_H(p_{\mathbf{d}, \mathbf{m}}, \pi_{\mathbf{d}, \mathbf{m}}) \leq \varepsilon$ .

To understand the key advantages granted by the tensor train approximation it suffices to consider the case of a uniform reference distribution on  $[0, 1]^{n_d+n_m}$  with density  $\rho_{\mathbf{d}, \mathbf{m}}^{\text{UNIF}}$ , and walk through the construction of the KR map  $\mathcal{T}$ . Making use of the component notation  $\mathbf{x}_{1:k} = (x_1, \dots, x_k)$ , note that the map  $\mathcal{S}: \mathbb{R}^{n_d+n_m} \rightarrow [0, 1]^{n_d+n_m}$  defined as  $\mathcal{S}(\mathbf{d}, \mathbf{m}) = [\mathcal{S}_d(\mathbf{d}), \mathcal{S}_{\mathbf{m}|\mathbf{d}}(\mathbf{d}, \mathbf{m})]^\top$  with components

$$(2.14) \quad \mathcal{S}_d(\mathbf{d}) = \begin{bmatrix} F_{d_1}(d_1) \\ F_{d_2|d_1}(d_1, d_2) \\ \vdots \\ F_{d_{n_d}|d_{1:n_d-1}}(\mathbf{d}_{n_d}) \end{bmatrix}$$

$$\text{and } \mathcal{S}_{\mathbf{m}|\mathbf{d}}(\mathbf{d}, \mathbf{m}) = \begin{bmatrix} F_{m_1|\mathbf{d}}(\mathbf{d}, m_1) \\ F_{m_2|\mathbf{d}, m_1}(\mathbf{d}, m_1, m_2) \\ \vdots \\ F_{m_{n_m}|\mathbf{d}, m_{1:n_m-1}}(\mathbf{d}, m_{1:n_m-1}, m_{n_m}) \end{bmatrix}$$

defines a triangular order-preserving coupling between the uniform reference and joint target such that  $\mathcal{S}_\# \pi_{\mathbf{d}, \mathbf{m}} = \rho_{\mathbf{d}, \mathbf{m}}^{\text{UNIF}}$ . Herein,

$$(2.15) \quad F_{z|\mathbf{y}}(\mathbf{y}, z) := \int_{-\infty}^z \pi_{z|\mathbf{y}}(z' | \mathbf{y}) \, dz' = \int_{-\infty}^z \frac{\pi_{\mathbf{y}, z}(\mathbf{y}, z')}{\pi_{\mathbf{y}}(\mathbf{y})} \, dz',$$

$$F_z(z) := \int_{-\infty}^z \pi_z(z') \, dz'$$

are cumulative distribution functions (CDFs). Through inversion of the map  $\mathcal{S}$ , we can define the map  $\mathcal{T} = \mathcal{S}^{-1}$  from (2.10) that pushes forward the uniform reference to the target,  $\mathcal{T}_\# \rho_{\mathbf{d}, \mathbf{m}}^{\text{UNIF}} = \pi_{\mathbf{d}, \mathbf{m}}$ . Thus, the key to realizing the KR map is the construction of the marginal densities  $\pi_{\mathbf{y}, z}$  in (2.15) (and hence the CDFs). This is precisely where the main advantage of the TT approximation becomes clear — the separable form of (2.11) enables dimension-by-dimension marginalization of  $p_{\mathbf{d}, \mathbf{m}} \approx \pi_{\mathbf{d}, \mathbf{m}}$  via a sequence of one-dimensional integrals. Replacing  $\pi_{\mathbf{y}, z}$  and  $\pi_{\mathbf{y}}$  in (2.15) with the corresponding marginalized tensor train approximations  $p_{\mathbf{y}, z}$  and  $p_{\mathbf{y}}$  then allows explicit definition of a transport map  $\tilde{\mathcal{T}}$  that pushes forward the reference to the *approximate* joint density, i. e.,  $\tilde{\mathcal{T}}_\# \rho_{\mathbf{d}, \mathbf{m}}^{\text{UNIF}} = p_{\mathbf{d}, \mathbf{m}} \approx \pi_{\mathbf{d}, \mathbf{m}}$ . In the remainder of this article, we drop the tilde and let  $\mathcal{T}$  be this approximate map.

The ability to construct a map  $\mathcal{S}$  between any target density and the standard uniform reference  $\rho_{\mathbf{d}, \mathbf{m}}^{\text{UNIF}}$  is sufficient for constructing a Knothe-Rosenblatt transport between the joint density of interest  $\pi_{\mathbf{d}, \mathbf{m}}$  and any arbitrary product-form reference density  $\rho_{\mathbf{d}, \mathbf{m}}$ . More precisely, given a diagonal map  $\mathcal{R}$  such that  $\mathcal{R}_\# \rho_{\mathbf{d}, \mathbf{m}}(\mathbf{u}_d, \mathbf{u}_m) = \rho_{\mathbf{d}, \mathbf{m}}^{\text{UNIF}}(\mathbf{u}_d, \mathbf{u}_m)$ , the composite map  $\mathcal{T} = \mathcal{S}^{-1} \circ \mathcal{R}$  defines a lower-triangular map satisfying the property  $\mathcal{T}_\# \rho_{\mathbf{d}, \mathbf{m}}(\mathbf{d}, \mathbf{m}) = p_{\mathbf{d}, \mathbf{m}}(\mathbf{d}, \mathbf{m})$ .

The method outlined in this section could be used to obtain straightforward approximations to the objective functions  $\Psi_A(\mathbf{e})$  and  $\Psi_D(\mathbf{e})$  in (2.7)–(2.8) for any fixed design  $\mathbf{e}$ . Specifically, one would need to build a KR map  $\mathcal{T}^e$  satisfying  $\mathcal{T}_\#^e \rho_{\mathbf{d}, \mathbf{m}}(\mathbf{d}, \mathbf{m}) = p_{\mathbf{d}, \mathbf{m}|\mathbf{e}}(\mathbf{d}, \mathbf{m})$ . Given this transport map, one could then define the SAAs  $\hat{\Psi}_A^N(\mathbf{e})$  and  $\hat{\Psi}_D^N(\mathbf{e})$  using samples from the approximate distributions for  $\mathbf{d} | \mathbf{e}$  as well as  $\mathbf{d}, \mathbf{m} | \mathbf{e}$ , and  $\mathbf{m} | \mathbf{e}, \mathbf{d}$ . However, since our goal is finding a design vector  $\mathbf{e}^*$  that maximizes these functions, the objective needs to be evaluated for potentially many designs, and a separate transport map would need to be built for each different design. Depending on the optimization procedure used, this could quickly get prohibitively expensive. Instead, in the following section, we present an alternative approach that enables us to approximate  $\Psi_A^N(\mathbf{e})$  and  $\Psi_D^N(\mathbf{e})$  for any design through the construction of only one KR map.

### 3. OED USING TRANSPORT MAPS

In this section we present a flexible transport map approach to OED for a wide class of Bayesian inverse problems using the ideas outlined in Section 2.3. The key to our approach (outlined in Section 3.1) is the construction of a transport map that couples the joint law of the parameter, observable *and*

experimental design random variables to a reference probability law. Some challenges in realizing such a KR rearrangement, as well as potential alleviations, are addressed in [Section 3.2](#). [Section 3.3](#) describes a few transport-map-based approximations to the OED objective function (2.4) with particular emphasis on A- and D-optimality.

**3.1. Knothe-Rosenblatt Rearrangement for OED.** At the core of our approach is the approximation of the joint density for the design, observable and inference parameter random variables,  $\pi_{\mathbf{e},\mathbf{d},\mathbf{m}}$ , by the pushforward of a product-form reference density  $\rho_{\mathbf{e},\mathbf{d},\mathbf{m}}(\mathbf{v}) = \rho_{\mathbf{e}}(v_e) \rho_{\mathbf{d}}(v_d) \rho_{\mathbf{m}}(v_m)$  under a KR transport map  $\mathcal{T}$ , i. e.,  $\mathcal{T}_\# \rho_{\mathbf{e},\mathbf{d},\mathbf{m}} = p_{\mathbf{e},\mathbf{d},\mathbf{m}} \approx \pi_{\mathbf{e},\mathbf{d},\mathbf{m}}$ . Using properties of conditional probability distributions and Bayes' law,  $\pi_{\mathbf{e},\mathbf{d},\mathbf{m}}(\mathbf{e}, \mathbf{d}, \mathbf{m}) = \pi_{\mathbf{d}|\mathbf{e},\mathbf{m}}(\mathbf{d} | \mathbf{e}, \mathbf{m}) \pi_{\mathbf{m}}(\mathbf{m}) \pi_{\mathbf{e}}(\mathbf{e})$ , where  $\pi_{\mathbf{d}|\mathbf{e},\mathbf{m}}$  is the design-dependent likelihood,  $\pi_{\mathbf{m}}$  is the prior, and  $\pi_{\mathbf{e}}$  is a user-specified density for the design parameters  $\mathbf{e}$ .

**Remark 3.1** (On the probability density for the designs). *We note that the marginal density on the designs  $\pi_{\mathbf{e}}$  is introduced as a consequence of the decomposition of the joint density  $\pi_{\mathbf{e},\mathbf{d},\mathbf{m}}$  into the product of conditional marginal densities. In general, there is no single “correct” fixed choice for  $\pi_{\mathbf{e}}$ . In particular, under our assumptions on the likelihood and prior, the posterior density is independent of the particular choice for  $\pi_{\mathbf{e}}$ . We defer making any specific choices to [Section 5](#). It is important, however, that the support of  $\pi_{\mathbf{e}}$  covers the space of possible designs  $\mathcal{E}$  and we assume this henceforth. Additionally, while the posterior is unchanged for different choices of  $\pi_{\mathbf{e}}$ , it does of course change the joint density. Therefore, the choice of  $\pi_{\mathbf{e}}$  may impact the performance of the FTT approximation to the joint density.*

The Knothe-Rosenblatt rearrangement for an arbitrary law on the random variables  $\mathbf{x} = (x_1, \dots, x_n)$  is unique once a particular arrangement of the variables is prescribed. While there are advantages to other arrangements of the variables (including ease of computation), we order the design, observable and inference parameter random variables as  $\mathbf{x} = (\mathbf{e}, \mathbf{d}, \mathbf{m})$ . The triangular KR map  $\mathcal{T}$  is then defined using the inverse of  $\mathcal{S}$ , where

$$(3.1) \quad \mathcal{S}(\mathbf{x}) = \begin{bmatrix} \mathcal{S}_{\mathbf{e}}(\mathbf{e}) \\ \mathcal{S}_{\mathbf{d}|\mathbf{e}}(\mathbf{e}, \mathbf{d}) \\ \mathcal{S}_{\mathbf{m}|\mathbf{e},\mathbf{d}}(\mathbf{e}, \mathbf{d}, \mathbf{m}) \end{bmatrix} = \begin{bmatrix} \mathbf{v}_{\mathbf{e}} \\ \mathbf{v}_{\mathbf{d}} \\ \mathbf{v}_{\mathbf{m}} \end{bmatrix} = \mathbf{v},$$

such that  $\mathcal{S}_\# p_{\mathbf{e},\mathbf{d},\mathbf{m}} = \rho_{\mathbf{e},\mathbf{d},\mathbf{m}}^{\text{UNIF}}$  for some  $p_{\mathbf{e},\mathbf{d},\mathbf{m}} \approx \pi_{\mathbf{e},\mathbf{d},\mathbf{m}}$ . The main advantage of using this particular arrangement over alternative orderings is the immediate access to the conditional distributions needed for defining the OED optimality criteria.

In particular, making use of the following notation for  $\mathcal{T} = \mathcal{S}^{-1} \circ \mathcal{R}$  (where  $\mathcal{R}$  again defines a coupling between the uniform density  $\rho_{\mathbf{e},\mathbf{d},\mathbf{m}}^{\text{UNIF}}$  and reference density  $\rho_{\mathbf{e},\mathbf{d},\mathbf{m}}$ ),

$$(3.2) \quad \mathcal{T}(\mathbf{v}) = \begin{bmatrix} \mathcal{T}_{\mathbf{e}}(\mathbf{v}_{\mathbf{e}}) \\ \mathcal{T}_{\mathbf{d}|\mathbf{e}}(\mathbf{v}_{\mathbf{e}}, \mathbf{v}_{\mathbf{d}}) \\ \mathcal{T}_{\mathbf{m}|\mathbf{e},\mathbf{d}}(\mathbf{v}_{\mathbf{e}}, \mathbf{v}_{\mathbf{d}}, \mathbf{v}_{\mathbf{m}}) \end{bmatrix} = \begin{bmatrix} \mathbf{e} \\ \mathbf{d} \\ \mathbf{m} \end{bmatrix},$$

we have

$$(3.3) \quad \begin{aligned} \begin{bmatrix} \mathbf{v}_{\mathbf{d}} \\ \mathbf{v}_{\mathbf{m}} \end{bmatrix} \sim \rho_{\mathbf{d},\mathbf{m}} &\Rightarrow \mathcal{T}_{\mathbf{d},\mathbf{m}|\mathbf{e}^*}(\mathbf{v}_{\mathbf{d}}, \mathbf{v}_{\mathbf{m}}) := \begin{bmatrix} \mathcal{T}_{\mathbf{d}|\mathbf{e}}(\mathbf{v}_{\mathbf{e}}^*, \mathbf{v}_{\mathbf{d}}) \\ \mathcal{T}_{\mathbf{m}|\mathbf{e},\mathbf{d}}(\mathbf{v}_{\mathbf{e}}^*, \mathbf{v}_{\mathbf{d}}, \mathbf{v}_{\mathbf{m}}) \end{bmatrix} \sim p_{\mathbf{d},\mathbf{m}|\mathbf{e}^*}, \\ \mathbf{v}_{\mathbf{m}} \sim \rho_{\mathbf{m}} &\Rightarrow \mathcal{T}_{\mathbf{m}|\mathbf{e}^*,\mathbf{d}^*}(\mathbf{v}_{\mathbf{m}}) := \mathcal{T}_{\mathbf{m}|\mathbf{e},\mathbf{d}}(\mathbf{v}_{\mathbf{e}}^*, \mathbf{v}_{\mathbf{d}}^*, \mathbf{m}) \sim p_{\mathbf{m}|\mathbf{e}^*,\mathbf{d}^*}, \end{aligned}$$

where  $\mathbf{v}_{\mathbf{e}}^* := \mathcal{T}_{\mathbf{e}}^{-1}(\mathbf{e}^*)$  and  $\mathbf{v}_{\mathbf{d}}^* := \mathcal{T}_{\mathbf{d}|\mathbf{e}}^{-1}(\mathbf{e}^*, \mathbf{d}^*)$ ; the inverse in the latter is taken with respect to the data variable  $\mathbf{d}$ . That is, through the operators  $\mathcal{T}_{\mathbf{d},\mathbf{m}|\mathbf{e}^*}$  and  $\mathcal{T}_{\mathbf{m}|\mathbf{e}^*,\mathbf{d}^*}$  we can obtain i. i. d. samples from and evaluate the approximations to the joint density  $p_{\mathbf{d},\mathbf{m}|\mathbf{e}^*} \approx \pi_{\mathbf{d},\mathbf{m}|\mathbf{e}^*}$  and posterior  $p_{\mathbf{m}|\mathbf{e}^*,\mathbf{d}^*} \approx \pi_{\mathbf{m}|\mathbf{e}^*,\mathbf{d}^*}$  for any design  $\mathbf{e}^* \in \mathcal{E}$ . These operators will be revisited in [Section 3.3](#) to define the transport-map-based approximations to the OED criteria. First we comment on the numerical construction of the KR map  $\mathcal{T}$ .

### 3.2. Construction of $\mathcal{T}$ for OED Using Tensor Trains and a Deep Composition of KR Maps.

To realize  $\mathcal{T}$  we use the tensor train (TT) approach to build  $\mathcal{S}$  as discussed in [Section 2.3](#). Given a

tensor train approximation  $g_{\mathbf{e}, \mathbf{d}, \mathbf{m}}$  to the square root of the joint density  $\pi_{\mathbf{e}, \mathbf{d}, \mathbf{m}}$ , we have

$$(3.4) \quad \pi_{\mathbf{e}, \mathbf{d}, \mathbf{m}}(\mathbf{e}, \mathbf{d}, \mathbf{m}) \approx p_{\mathbf{e}, \mathbf{d}, \mathbf{m}}(\mathbf{e}, \mathbf{d}, \mathbf{m}) \propto g_{\mathbf{e}, \mathbf{d}, \mathbf{m}}(\mathbf{e}, \mathbf{d}, \mathbf{m})^2 = \left( \prod_{i=1}^n \tilde{\mathbf{G}}_i(x_i) \right)^2,$$

where  $\mathbf{x} := (\mathbf{e}, \mathbf{d}, \mathbf{m}) \in \mathbb{R}^n = \mathbb{R}^{n_e + n_d + n_m}$  and  $\tilde{\mathbf{G}}_i \in \mathbb{R}^{r_{i-1} \times r_i}$  denotes the  $i$ -th tensor train core,

$$\tilde{\mathbf{G}}_i(x_i) := \begin{cases} \mathbf{G}_{e_i}(e_i) & \text{if } i \in [1, n_e], \\ \mathbf{G}_{d_{i-n_e}}(d_{i-n_e}) & \text{if } i \in [n_e + 1, n_e + n_d], \\ \mathbf{G}_{m_{i-(n_e+n_d)}}(m_{i-(n_e+n_d)}) & \text{if } i \in [n_e + n_d + 1, n_e + n_d + n_m]. \end{cases}$$

The components of  $\mathcal{S}$  are then defined analogously to (2.14), where for any choice of variables  $z$  and  $\mathbf{y}$  (e.g.,  $z = d_k$ ,  $\mathbf{y} = \mathbf{e}$ ,  $\mathbf{d}_{1:k-1}$ ), the cumulative marginalized conditional density functions  $F_{z|\mathbf{y}}(\mathbf{y}, z)$  are defined using (2.15). As mentioned previously, for all positive integers  $k < n = n_e + n_d + n_m$ , the marginal densities  $p_{\mathbf{x}_{1:k}}$  for the random variables  $\mathbf{x}_{1:k} = (x_1, \dots, x_k)$  satisfy

$$(3.5) \quad p_{\mathbf{x}_{1:k}}(\mathbf{x}_{1:k}) = \int p_{\mathbf{x}}(\mathbf{x}_{1:k}, \mathbf{x}_{k+1:n}) \, d\mathbf{x}_{k+1:n}$$

and can be computed recursively dimension-by-dimension using a sequence of one-dimensional integrals starting with the last variable  $x_n = m_{n_m}$ .

Typically, the computational bottleneck of constructing functional tensor trains (FTTs) for problems where the PTO map involves discretized PDE/ODE solves is the evaluation of the unnormalized density since each evaluation requires solving the aforementioned PDE/ODE. Thus, as hinted by (2.12), the computational efficiency or feasibility of constructing  $\mathcal{T}$  is highly dependent on the ranks or dimensions of the matrices  $\tilde{\mathbf{G}}_i$ . For certain problems this bottleneck could be mitigated by employing a reduced-order model surrogate to the parameter-to-observable map. However, a sufficiently accurate surrogate may not be available for certain problems, or may still be rather expensive to evaluate. In general keeping the ranks as small as possible (while maintaining accuracy of the approximation) is vital to the efficiency of the algorithm.

Unfortunately for certain “complicated” density functions, tensor train decompositions as proposed in [24] may require very large ranks to ensure  $\mathcal{D}_H(p_{\mathbf{e}, \mathbf{d}, \mathbf{m}}, \pi_{\mathbf{e}, \mathbf{d}, \mathbf{m}}) \leq \varepsilon$  for suitably small error tolerance  $\varepsilon$ . Examples of such “complicated” densities include those exhibiting complex nonlinear correlation structures or those concentrated to a small region in the domain. Particularly due to the interaction of the design and observable variables, the joint densities of interest  $\pi_{\mathbf{e}, \mathbf{d}, \mathbf{m}}$  tend to exhibit such characteristics.

For an illustrative example, consider a linear inverse problem governed by Poisson’s equation  $-u_{xx} = m_1 \sin(\frac{4}{3}x) + m_2 \cos(2x)$  with constant Dirichlet data prescribed at the boundaries of the domain interval  $\Omega := (0, 2\pi)$ . As the design problem, the location  $e \in \Omega$  where the state  $u$  should be measured is to be chosen such that the inference of the parameter  $\mathbf{m} = [m_1, m_2]$  is optimized. Despite the Gaussian likelihood and posterior, the joint density  $\pi_{\mathbf{e}, \mathbf{d}}$  (visualized in Figure 3.1) is non-Gaussian even in this simple toy example. In particular, the density has multiple sharp peaks and concentrates along the diagonal. These characteristics make it challenging to construct a sufficiently accurate TT approximation to  $\pi_{\mathbf{e}, \mathbf{d}, \mathbf{m}}$  in one step.

To alleviate the challenges presented by such complex densities, in [19], the authors propose the *deep inverse Rosenblatt transport* (DIRT), a procedure that builds a composition of transport maps guided by a suitable sequence of bridging measures. Given a sequence of  $L + 1$  bridging densities  $\{\pi_{\mathbf{e}, \mathbf{d}, \mathbf{m}}^\ell\}_{\ell=0}^L$  that gradually capture the complexity of the joint target density with  $\pi_{\mathbf{e}, \mathbf{d}, \mathbf{m}}^L := \pi_{\mathbf{e}, \mathbf{d}, \mathbf{m}}$ , the full composite transport map satisfying  $\mathcal{T}_\# \rho_{\mathbf{e}, \mathbf{d}, \mathbf{m}} = p_{\mathbf{e}, \mathbf{d}, \mathbf{m}}$  is defined as

$$(3.6) \quad \mathcal{T} := \mathcal{T}_L = \mathcal{Q}_0 \circ \mathcal{Q}_1 \circ \dots \circ \mathcal{Q}_L.$$

For each  $0 \leq \ell \leq L$ , the composite transport map  $\mathcal{T}_\ell = \mathcal{Q}_0 \circ \dots \circ \mathcal{Q}_\ell$  provides an approximation to the  $\ell$ -th bridging density, i.e.,  $(\mathcal{T}_\ell)_\# \rho_{\mathbf{e}, \mathbf{d}, \mathbf{m}} = p_{\mathbf{e}, \mathbf{d}, \mathbf{m}}^\ell \approx \pi_{\mathbf{e}, \mathbf{d}, \mathbf{m}}^\ell$ .

The intermediate maps are constructed sequentially in a greedy fashion. At stage  $\ell + 1$ , assuming  $\mathcal{T}_\ell$  is built, the next layer  $\mathcal{Q}_{\ell+1}$  is constructed as a KR map satisfying  $(\mathcal{Q}_{\ell+1})_\# \rho_{\mathbf{e}, \mathbf{d}, \mathbf{m}} = q_{\mathbf{e}, \mathbf{d}, \mathbf{m}}^{\ell+1} \approx \mathcal{T}_\ell^\# \pi_{\mathbf{e}, \mathbf{d}, \mathbf{m}}^{\ell+1}$ . This procedure can be seen as a successive change of coordinates or as a preconditioning procedure.

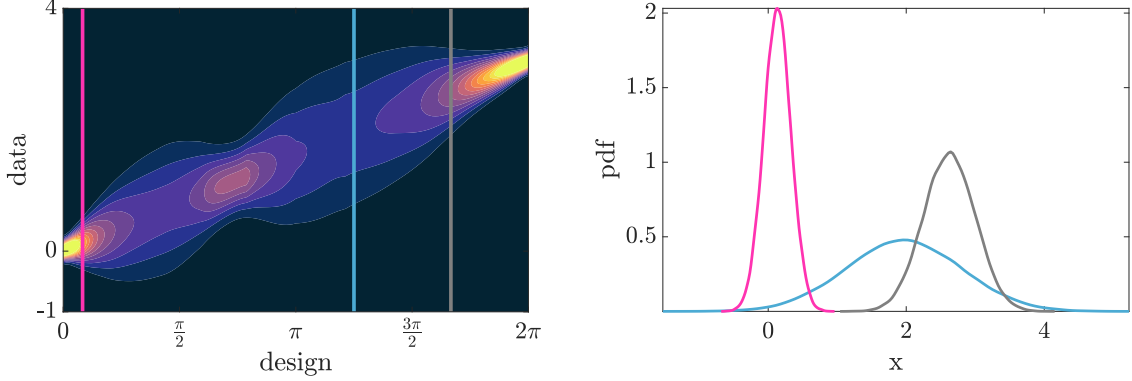


FIGURE 3.1. On the left, a filled contour plot of a two-dimensional density  $\pi_{e,d}$  for the illustrative toy problem in Section 3.2. A visualization of  $\pi_{d|e^*}$  for three different design locations  $e^*$  is visualized in the right image. The three different designs correspond to the vertical color-coded lines overlaid on the contour plot in the left.

At each stage, the previous composite map  $\mathcal{T}_\ell$  is used to precondition the next bridging density. If the adjacent bridging densities  $\pi_{e,d,m}^\ell$  and  $\pi_{e,d,m}^{\ell+1}$  are close enough in some sense, e. g., with respect to the Hellinger distance, then the map  $\mathcal{T}_\ell$  is capable of capturing some of the correlation structures of  $\pi_{e,d,m}^{\ell+1}$  and the preconditioned density  $\mathcal{T}_\ell^\# \pi_{e,d,m}^{\ell+1}$  is easier to approximate in tensor train format than  $\pi_{e,d,m}^{\ell+1}$ .

Unsurprisingly, the accuracy of the final composite map surrogate depends on similarity measures between adjacent bridging densities. Under relatively mild assumptions on the bridging densities  $\pi_{e,d,m}^\ell$  and the maps  $\mathcal{Q}_\ell$  for  $\ell = 0, \dots, L$ , specifically that

$$(3.7) \quad \begin{aligned} \sup_{0 \leq \ell < L} \mathcal{D}_H(\pi_{e,d,m}^\ell, \pi_{e,d,m}^{\ell+1}) &\leq \eta, \\ \mathcal{D}_H((\mathcal{Q}_0)_\# \rho_{e,d,m}, \pi_{e,d,m}^0) &\leq \omega \eta \end{aligned}$$

for some positive  $\eta < 1$  and  $\omega \in [0, 1)$ , and that each  $\mathcal{Q}_{\ell+1}$  (for  $\ell < L$ ) reduces the approximation error such that

$$(3.8) \quad \mathcal{D}_H((\mathcal{Q}_{\ell+1})_\# \rho_{e,d,m}, \mathcal{T}_\ell^\# \pi_{e,d,m}^{\ell+1}) \leq \omega \mathcal{D}_H(\rho_{e,d,m}, \mathcal{T}_\ell^\# \pi_{e,d,m}^{\ell+1}),$$

it is shown in [19] and [20] that the Hellinger distance between the target density and its surrogate approximation  $p_{e,d,m} = \mathcal{T}_\# \rho_{e,d,m}$  satisfies

$$(3.9) \quad \mathcal{D}_H(p_{e,d,m}, \pi_{e,d,m}) \leq \varepsilon = \frac{\omega}{1-\omega} \eta.$$

Additionally, the following proposition provides a probabilistic bound on the approximation error to the conditional densities  $\pi_{d,m|e}$  and  $\pi_{m|e,d}$  using the conditional transport maps  $\mathcal{T}_{d,m|e}$  and  $\mathcal{T}_{m|e,d}$  (as defined in (3.3)).

**Proposition 3.2** (Probabilistic error bound on conditional densities, [20, Appendix A.2]). *Using the ordering-preserving partition  $(z, y) = (e, d, m)$ , if  $p_{z,y} \approx \pi_{z,y}$  with  $\mathcal{D}_H(\pi_{z,y}, p_{z,y}) \leq \varepsilon$  holds, then for any  $\delta \in [0, 1]$ ,*

$$\mathbb{P}_{\pi_z} [\mathcal{D}_H(\pi_{y|z}, p_{y|z}) \leq \delta] \geq 1 - \frac{2\varepsilon}{\delta}.$$

The bridging densities can be defined in various ways and what constitutes a smart choice is problem-dependent. One generally suitable option is the *tempering* approach [27]. Given a sequence of temperatures  $0 = \beta_0 < \beta_1 < \dots < \beta_L = 1$ , the  $\ell$ -th tempered bridging density can be defined as  $\pi_{e,d,m}^\ell = \left( \frac{\pi_{e,d,m}}{\rho_{e,d,m}} \right)^{\beta_\ell} \rho_{e,d,m}$  or  $\pi_{e,d,m}^\ell = (\pi_{e,d,m})^{\beta_\ell}$ . Alternatively, in the case of Bayesian inference, if one is interested in approximating a highly concentrated posterior density stemming from an inverse

problem with a large amount of data, it may be beneficial to build the bridging densities by adding the data sequentially in batches as  $l$  increases.

Once a suitable sequence of bridging densities is chosen that satisfies (3.7), the inequalities (3.8) pave the way for constructing the intermediate layers  $\mathcal{Q}_\ell$ . The KR maps at each layer can be constructed using the procedure outlined in the beginning of this section, i.e., via a tensor train approximation to the square root of the pullback of the  $\ell$ -th bridging density. To ease readability of the OED algorithms presented in the subsequent sections, we reproduce the DIRT algorithm in [Algorithm 1](#).

---

**Algorithm 1** Deep Inverse Rosenblatt Transport (DIRT) [19].

---

```

1: procedure DIRT( $\rho_{e,d,m}, \{\pi_{e,d,m}^\ell\}_{\ell=0}^L, \varepsilon$ )
   #  $\varepsilon \leq \omega \eta$ , with  $\omega, \eta$  satisfying (3.7)
2:    $g_{e,d,m}^0 \leftarrow$  TT approx. to  $(\pi_{e,d,m}^0)^{1/2}$  s. t.  $\|(\pi_{e,d,m}^0)^{1/2} - g_{e,d,m}^0\|_{L_2} \leq \frac{\varepsilon}{\sqrt{2}}$ 
3:    $\mathcal{T}_0 \leftarrow$  inverse KR map satisfying  $\mathcal{D}_H((\mathcal{T}_0)_\# \rho_{e,d,m}, \pi_{e,d,m}^0) \leq \varepsilon$ 
4:   for  $\ell = 1, \dots, L$  do
5:      $g_{e,d,m}^\ell \leftarrow$  TT approx. to  $(\pi_{e,d,m}^\ell)^{1/2}$  s. t.  $\|(\pi_{e,d,m}^\ell)^{1/2} - g_{e,d,m}^\ell\|_{L_2} \leq \frac{\varepsilon}{\sqrt{2}}$ 
6:      $\mathcal{Q}_\ell \leftarrow$  inverse KR map satisfying  $\mathcal{D}_H((\mathcal{Q}_\ell)_\# \rho_{e,d,m}, \mathcal{T}_{\ell-1}^\# \pi_{e,d,m}^\ell) \leq \varepsilon$ 
7:      $\mathcal{T}_\ell \leftarrow \mathcal{T}_{\ell-1} \circ \mathcal{Q}_\ell$ 
8:   end for
9:   return  $\mathcal{T}_\ell$ 
10: end procedure

```

---

**3.3. Approximation of Optimality Criteria Using KR Maps.** Recall that our OED objective is to find a design  $e^* \in \mathcal{E}$  that maximizes an expected utility function  $\Psi$ ,

$$e^* \in \underset{e \in \mathcal{E}}{\text{Arg max}} \Psi(e) = \underset{e \in \mathcal{E}}{\text{Arg max}} \mathbb{E}_{\pi_{d|e}} [\psi(e, \mathbf{d})].$$

The most evident way to make use of the transport-map-based surrogate to the joint density  $\pi_{e,d,m}$  is through a direct replacement of all the conditional densities required for defining  $\Psi$  with their corresponding transport map-based surrogates. The resulting approximate optimality criterion  $\hat{\Psi}$  can then be approximated using Monte Carlo or Quasi-Monte Carlo quadrature.

For example, using the operators  $\mathcal{T}_{d,m|e}$  and  $\mathcal{T}_{m|e,d}$  in (3.3) to define  $p_{d,m|e} = (\mathcal{T}_{d,m|e})_\# \rho_{d,m}$  and  $p_{m|e,d} = (\mathcal{T}_{m|e,d})_\# \rho_m$ , we propose the following SAA approximations to the A- and D-optimal design objectives.

**A-Optimal Design Objective.** We consider

$$\begin{aligned}
(3.10) \quad \Psi_A(e) &= -\mathbb{E}_{\pi_{d|e}} [\text{trace}(\mathbf{C}_{m|e,d}(e, \mathbf{d}))] \\
&\approx -\frac{1}{N} \sum_{i=1}^N \sum_{j=1}^{n_m} \widehat{\text{Var}}_{p_{m|e,d^{(i)}}}(m_j) =: \widehat{\Psi}_A^N(e),
\end{aligned}$$

where  $\mathbf{d}^{(i)} \sim p_{d|e}$ , and

$$\widehat{\text{Var}}_{p_{m|e,d^{(i)}}}(m_j) \approx \widehat{\text{Var}}_{p_{m|e,d^{(i)}}}(m_j) := \frac{1}{M-1} \sum_{k=1}^M (m_j^{(k,i)} - \bar{m}_j^{(i)})^2$$

with  $\mathbf{m}^{(k,i)} \sim p_{m|e,d^{(i)}}$  and  $\bar{m}_j^{(i)} := \frac{1}{M} \sum_{k=1}^M m_j^{(k,i)}$  is the sample-based approximation to the posterior variance. For the numerical results in [Section 5](#), we use Quasi-Monte Carlo to approximate the outer expectation with respect to the evidence  $p_{d|e}$  and use the transport map  $\mathcal{T}_{m|e,d^{(i)}}$  to push forward  $M$  randomly drawn samples  $\mathbf{v}_m^{(k)} \sim \rho_m$  for each sample  $\mathbf{d}^{(i)}$ . The posterior variance is then calculated using the samples  $\mathbf{m}^{(k,i)} = \mathcal{T}_{m|e,d^{(i)}}(\mathbf{v}_m^{(k)})$ . The full procedure for evaluating  $\widehat{\Psi}_A^N(e)$  for any design  $e \in \mathcal{E}$  is summarized in [Algorithm 2](#).

---

**Algorithm 2** Evaluate  $\widehat{\Psi}_A^N(\mathbf{e}) \approx \Psi_A(\mathbf{e})$  using transport map to joint density.

---

```

1: procedure AOPT( $\rho_{\mathbf{e},\mathbf{d},\mathbf{m}}, \mathcal{T}, \mathbf{e}, N, M$ ) #  $\mathcal{T}_{\#} \rho_{\mathbf{e},\mathbf{d},\mathbf{m}} \approx \pi_{\mathbf{e},\mathbf{d},\mathbf{m}}$ 
2:   Quasi-random  $\mathbf{v}_d^{(i)} \sim \rho_{\mathbf{d}}$  for  $i = 1, \dots, N$  generated using the Sobol sequence
3:    $\mathbf{d}^{(i)} \leftarrow \mathcal{T}_{\mathbf{d}|\mathbf{e}}(\mathbf{v}_d^{(i)})$  for  $i = 1, \dots, N$ 
4:   Sample  $\mathbf{v}_m^{(k)} \sim \rho_{\mathbf{m}}$  for  $k = 1, \dots, M$ 
5:   for  $i=1, \dots, N$  do
6:      $\mathbf{m}^{(k,i)} \leftarrow \mathcal{T}_{\mathbf{m}|\mathbf{e},\mathbf{d}^{(i)}}(\mathbf{v}_m^{(k)})$  for  $k = 1, \dots, M$ 
7:      $\psi_A(\mathbf{e}, \mathbf{d}^{(i)}) \leftarrow \sum_{j=1}^{n_m} \widehat{\text{Var}}(m_j^{(k,i)})$  #  $\mathbf{m}^{(k,i)} = [m_1^{(k,i)}, \dots, m_{n_m}^{(k,i)}]$ 
8:   end for
9:    $\widehat{\Psi}_A^N \leftarrow \frac{1}{N} \sum_{i=1}^N \psi_A(\mathbf{e}, \mathbf{d}^{(i)})$ 
10:  return  $\widehat{\Psi}_A^N(\mathbf{e})$ 
11: end procedure

```

---

**D-Optimal Design Objective.** We use

$$\begin{aligned}
(3.11) \quad \Psi_D(\mathbf{e}) &= \mathbb{E}_{\pi_{\mathbf{d},\mathbf{m}|\mathbf{e}}} \left[ \log \left( \frac{\pi_{\mathbf{m}|\mathbf{e},\mathbf{d}}}{\pi_{\mathbf{m}}} \right) \right] \\
&\approx \frac{1}{N} \sum_{i=1}^N \log \left( \frac{p_{\mathbf{m}|\mathbf{e},\mathbf{d}}(\mathbf{m}^{(i)} | \mathbf{e}, \mathbf{d}^{(i)})}{\pi_{\mathbf{m}}(\mathbf{m}^{(i)})} \right) =: \widehat{\Psi}_D^N(\mathbf{e}),
\end{aligned}$$

where  $(\mathbf{d}^{(i)}, \mathbf{m}^{(i)}) \sim p_{\mathbf{d},\mathbf{m}|\mathbf{e}}$ . Algorithm 3 summarizes the procedure for evaluating  $\widehat{\Psi}_D^N(\mathbf{e})$  for any  $\mathbf{e} \in \mathcal{E}$ .

---

**Algorithm 3** Evaluate  $\widehat{\Psi}_D^N(\mathbf{e}) \approx \Psi_D(\mathbf{e})$  using transport map to joint density.

---

```

1: procedure DOPT( $\rho_{\mathbf{e},\mathbf{d},\mathbf{m}}, \mathcal{T}, \pi_{\mathbf{m}}, \mathbf{e}, N$ ) #  $\mathcal{T}_{\#} \rho_{\mathbf{e},\mathbf{d},\mathbf{m}} \approx \pi_{\mathbf{e},\mathbf{d},\mathbf{m}}$ 
2:   Sample  $\mathbf{v}_d^{(i)}, \mathbf{v}_m^{(i)} \sim \rho_{\mathbf{d},\mathbf{m}}$  for  $i = 1, \dots, N$ 
3:    $\mathbf{d}^{(i)}, \mathbf{m}^{(i)} \leftarrow \mathcal{T}_{\mathbf{d},\mathbf{m}|\mathbf{e}}(\mathbf{v}_d^{(i)}, \mathbf{v}_m^{(i)})$  for  $i = 1, \dots, N$ 
4:   for  $i=1, \dots, N$  do
5:      $p_{\mathbf{m}|\mathbf{e},\mathbf{d}^{(i)}}(\mathbf{m}^{(i)}) = (\mathcal{T}_{\mathbf{m}|\mathbf{e},\mathbf{d}^{(i)}})_{\#} \rho_{\mathbf{m}}(\mathbf{m}^{(i)})$  #  $\mathcal{T}_{\mathbf{m}|\mathbf{d}^i, \mathbf{e}}$  defined in (3.3)
6:      $\psi_D(\mathbf{e}, \mathbf{d}^{(i)}, \mathbf{m}^{(i)}) \leftarrow \log \left( \frac{p_{\mathbf{m}|\mathbf{e},\mathbf{d}^{(i)}}(\mathbf{m}^{(i)})}{\pi_{\mathbf{m}}(\mathbf{m}^{(i)})} \right)$ 
7:   end for
8:    $\widehat{\Psi}_D^N(\mathbf{e}) \leftarrow \frac{1}{N} \sum_{i=1}^N \psi_D(\mathbf{e}, \mathbf{d}^{(i)}, \mathbf{m}^{(i)})$ 
9:   return  $\widehat{\Psi}_D^N(\mathbf{e})$ 
10: end procedure

```

---

With these Monte Carlo approximations to  $\Psi_X$  (for  $X = A, D$ ), the OED goal reduces to finding a design vector  $\mathbf{e}^*$  maximizing the tractable approximate expected utility function

$$(3.12) \quad \mathbf{e}^* \in \underset{\mathbf{e} \in \mathcal{E}}{\text{Arg max}} \widehat{\Psi}_X^N(\mathbf{e}).$$

A detailed discussion of viable algorithms for optimizing  $\widehat{\Psi}_X^N$  is outside the scope of this work. For the numerical results presented in Section 5, we use gradient-free optimization approaches, thus we do not derive the gradients of  $\widehat{\Psi}_X^N$ . Of course, gradient-based optimizers can also be used, provided  $\widehat{\Psi}_X^N(\mathbf{e})$  is differentiable with respect to  $\mathbf{e}$ . We leave the choice of optimization algorithm to be a black box that can be specified by the reader, and summarize the full transport-map-based procedure for finding designs maximizing  $\widehat{\Psi}_X^N$  in Algorithm 4.

---

**Algorithm 4** OED using the transport-map-based SAAs  $\widehat{\Psi}_X^N \approx \Psi_X$ .

---

```

1: procedure OED( $\rho_{e,d,m}, \pi_{e,d,m}, \pi_m, E, X, \varepsilon, N$ )
2:   Choose bridging densities  $\{\pi_{e,d,m}^\ell\}_{\ell=0}^L$ 
3:    $\mathcal{T} \leftarrow \text{DIRT}(\rho_{e,d,m}, \{\pi_{e,d,m}^\ell\}_{\ell=0}^L, \varepsilon)$ 
4:   if  $X = D$  then # D-optimal designs
5:     Choose  $e^* \in \text{Arg max}_{e \in \mathcal{E}} \text{DOpt}(\rho_{e,d,m}, \mathcal{T}, \pi_m, e, N)$ 
6:   end if
7:   if  $X = A$  then # A-optimal designs
8:     Choose number of inner samples  $M$ 
9:     Choose  $e^* \in \text{Arg max}_{e \in \mathcal{E}} \text{AOpt}(\rho_{e,d,m}, \mathcal{T}, e, N, M)$ 
10:  end if
11:  return  $e^*$ 
12: end procedure

```

---

**3.4. Error Bounds on the Transport Map-Based Approximation of the Expected Utility Function  $\Psi_X$ .** In the following, we derive probabilistic bounds for the error due to the approximation of an optimality criterion  $\Psi_X$  with the corresponding transport map-based surrogate. That is, for any  $\zeta > 0$ , we provide a lower bound for

$$(3.13) \quad \mathbb{P}_{\pi_e} \left[ \left| \Psi_X(e) - \widehat{\Psi}_X(e) \right| \leq \zeta \right],$$

where  $|\Psi_X(e) - \widehat{\Psi}_X(e)| := |\mathbb{E}_{\pi_{d,m|e}}[h] - \mathbb{E}_{p_{d,m|e}}[\widehat{h}]|$  with  $h(e, \mathbf{d}, \mathbf{m}) := g(\pi_{\mathbf{m}|e,d})$  and  $\widehat{h}(e, \mathbf{d}, \mathbf{m}) := g(p_{\mathbf{m}|e,d})$  for some measurable function  $g$  that depends on the optimality criterion. For illustrative purposes, we focus on the D-optimality criterion here, which corresponds to

$$(3.14) \quad h(e, \mathbf{d}, \mathbf{m}) := \log \left( \frac{\pi_{\mathbf{m}|e,d}}{\pi_{\mathbf{m}}} \right) \quad \text{and} \quad \widehat{h}(e, \mathbf{d}, \mathbf{m}) := \log \left( \frac{p_{\mathbf{m}|e,d}}{\pi_{\mathbf{m}}} \right).$$

The bounds for the A-optimality criterion can be derived using similar ideas.

To derive the lower bound, we make use of the following lemmas, the first of which concerns arbitrary PDFs of a random variable  $\mathbf{x}$  taking values in  $\mathcal{X} \subseteq \mathbb{R}^{n_x}$  for some  $n_x \in \mathbb{N}$ . To ease readability, we define

$$L_\pi^2(\mathcal{X}) := \{h: \mathcal{X} \rightarrow \mathbb{R} \mid h \text{ is measurable and } \|h\|_{L_\pi^2} < \infty\}$$

where

$$\|h\|_{L_\pi^2} := \sqrt{\mathbb{E}_\pi[h^2]}.$$

**Lemma 3.3** ([19, Proposition 6]). *Let  $\pi$  and  $p$  be two PDFs. For any function  $h \in L_\pi^2(\mathcal{X}) \cap L_p^2(\mathcal{X})$ ,*

$$(3.15) \quad \left| \mathbb{E}_\pi[h] - \mathbb{E}_p[h] \right| \leq \sqrt{2} \mathcal{D}_H(\pi, p) \left( \|h\|_{L_\pi^2} + \|h\|_{L_p^2} \right).$$

**Lemma 3.4.** *Let the ratio of two PDFs  $\pi$  and  $p$  be bounded from above almost surely, i. e.,*

$$(3.16) \quad \sup_{\mathbf{x} \in \mathcal{X} \subseteq \mathbb{R}^{n_x}} \frac{\pi(\mathbf{x})}{p(\mathbf{x})} \leq c < \infty.$$

*Then the KL divergence of  $\pi$  from  $p$  can be bounded as follows:*

$$(3.17) \quad \mathcal{D}_{\text{KL}}(\pi \| p) \leq \sqrt{2} \mathcal{D}_H(\pi, p) \left( \left\| \frac{\pi}{p} \right\|_{L_\pi^2} + \left\| \frac{\pi}{p} \right\|_{L_p^2} \right).$$

*Proof.* Under our assumptions, using [28, Theorem 5],  $\mathcal{D}_{\text{KL}}(\pi \| p) \leq \mathcal{D}_{\chi^2}(\pi \| p)$  where  $\mathcal{D}_{\chi^2}(\pi \| p)$  denotes the  $\chi^2$ -divergence of  $\pi$  from  $p$ . The statement then follows from [19, Corollary 2].  $\square$

**Lemma 3.5, Proposition 3.6, and Proposition 3.7** concern two probability densities  $\pi_{\mathbf{x},\mathbf{y}} = \pi_{\mathbf{x}|\mathbf{y}}\pi_{\mathbf{y}}$  and  $p_{\mathbf{x},\mathbf{y}} = p_{\mathbf{x}|\mathbf{y}}p_{\mathbf{y}}$  defined on  $\mathcal{X} \times \mathcal{Y} \subseteq \mathbb{R}^{n_x} \times \mathbb{R}^{n_y}$  (with  $n_x, n_y \in \mathbb{N}$ ).

**Lemma 3.5** ([20, Lemma 4]). *The expected value of the Hellinger distance between  $\pi_{\mathbf{x}|\mathbf{y}}$  and  $p_{\mathbf{x}|\mathbf{y}}$  satisfies:*

$$(3.18) \quad \mathbb{E}_{\pi_{\mathbf{y}}} \left[ \mathcal{D}_{\text{H}}(\pi_{\mathbf{x}|\mathbf{y}}, p_{\mathbf{x}|\mathbf{y}}) \right] \leq 2 \mathcal{D}_{\text{H}}(\pi_{\mathbf{x},\mathbf{y}}, p_{\mathbf{x},\mathbf{y}}).$$

Furthermore,

$$(3.19) \quad \mathbb{E}_{\pi_{\mathbf{y}}} \left[ \mathcal{D}_{\text{H}}(\pi_{\mathbf{x}|\mathbf{y}}, p_{\mathbf{x}|\mathbf{y}})^2 \right] \leq 4 \mathcal{D}_{\text{H}}(\pi_{\mathbf{x},\mathbf{y}}, p_{\mathbf{x},\mathbf{y}})^2.$$

**Proposition 3.6.** *Assume the PDFs  $\pi_{\mathbf{x},\mathbf{y}}$  and  $p_{\mathbf{x},\mathbf{y}}$  satisfy  $\mathcal{D}_{\text{H}}(\pi_{\mathbf{x},\mathbf{y}}, p_{\mathbf{x},\mathbf{y}}) \leq \varepsilon$  for some  $\varepsilon \geq 0$ . Furthermore, assume that the ratio of the conditional densities  $\pi_{\mathbf{x}|\mathbf{y}}$  and  $p_{\mathbf{x}|\mathbf{y}}$  is bounded almost surely by  $c_1 \in L^2_{\pi_{\mathbf{y}}}(\mathcal{Y})$ , i. e., for all  $\mathbf{y} \in \mathcal{Y}$ ,*

$$(3.20) \quad \sup_{\mathbf{x} \in \mathcal{X}} \frac{\pi_{\mathbf{x}|\mathbf{y}}(\mathbf{x})}{p_{\mathbf{x}|\mathbf{y}}(\mathbf{x})} \leq c_1(\mathbf{y}).$$

Then we have the following bound on the expected error:

$$(3.21) \quad \mathbb{E}_{\pi_{\mathbf{x},\mathbf{y}}} \left[ \log \left( \frac{\pi_{\mathbf{x}|\mathbf{y}}}{p_{\mathbf{x}|\mathbf{y}}} \right) \right] \leq 4 \sqrt{2} \varepsilon \|c_1\|_{L^2_{\pi_{\mathbf{y}}}}.$$

*Proof.* Note that

$$\begin{aligned} \mathbb{E}_{\pi_{\mathbf{x},\mathbf{y}}} \left[ \log \left( \frac{\pi_{\mathbf{x}|\mathbf{y}}}{p_{\mathbf{x}|\mathbf{y}}} \right) \right] &= \mathbb{E}_{\pi_{\mathbf{y}}} \left[ \mathbb{E}_{\pi_{\mathbf{x}|\mathbf{y}}} \left[ \log \left( \frac{\pi_{\mathbf{x}|\mathbf{y}}}{p_{\mathbf{x}|\mathbf{y}}} \right) \right] \right] \\ &= \mathbb{E}_{\pi_{\mathbf{y}}} \left[ \mathcal{D}_{\text{KL}}(\pi_{\mathbf{x}|\mathbf{y}} \| p_{\mathbf{x}|\mathbf{y}}) \right] \leq 2 \sqrt{2} \mathbb{E}_{\pi_{\mathbf{y}}} \left[ c_1(\mathbf{y}) \mathcal{D}_{\text{H}}(\pi_{\mathbf{x}|\mathbf{y}}, p_{\mathbf{x}|\mathbf{y}}) \right], \end{aligned}$$

where the inequality follows from Lemma 3.4 and assumption (3.20). Then, using Hölder's inequality and Lemma 3.5, we have:

$$\mathbb{E}_{\pi_{\mathbf{y}}} \left[ c_1(\mathbf{y}) \mathcal{D}_{\text{H}}(\pi_{\mathbf{x}|\mathbf{y}}, p_{\mathbf{x}|\mathbf{y}}) \right] \leq 2 \mathcal{D}_{\text{H}}(\pi_{\mathbf{x},\mathbf{y}}, p_{\mathbf{x},\mathbf{y}}) \|c_1\|_{L^2_{\pi_{\mathbf{y}}}},$$

and the result (3.21) thus follows.  $\square$

**Proposition 3.7.** *Let  $\pi_{\mathbf{x},\mathbf{y}}$  and  $p_{\mathbf{x},\mathbf{y}}$  be two PDFs satisfying  $\mathcal{D}_{\text{H}}(\pi_{\mathbf{x},\mathbf{y}}, p_{\mathbf{x},\mathbf{y}}) \leq \varepsilon$  for some  $\varepsilon \geq 0$ . Assume that the function  $\hat{h}(\mathbf{y}, \cdot)$  is bounded almost surely from above by  $c_2(\mathbf{y})$  with  $c_2 \in L^2_{\pi_{\mathbf{y}}}(\mathcal{Y})$ , i. e., for all  $\mathbf{y} \in \mathcal{Y}$ ,*

$$(3.22) \quad \sup_{\mathbf{x} \in \mathcal{X}} |\hat{h}(\mathbf{y}, \mathbf{x})| \leq c_2(\mathbf{y}).$$

Then

$$(3.23) \quad \mathbb{E}_{\pi_{\mathbf{y}}} \left[ \left| \mathbb{E}_{\pi_{\mathbf{x}|\mathbf{y}}}[\hat{h}] - \mathbb{E}_{p_{\mathbf{x}|\mathbf{y}}}[\hat{h}] \right| \right] \leq 4 \sqrt{2} \varepsilon \|c_2\|_{L^2_{\pi_{\mathbf{y}}}}.$$

*Proof.* Using Lemma 3.3, we have that

$$\mathbb{E}_{\pi_{\mathbf{y}}} \left[ \left| \mathbb{E}_{\pi_{\mathbf{x}|\mathbf{y}}}[\hat{h}] - \mathbb{E}_{p_{\mathbf{x}|\mathbf{y}}}[\hat{h}] \right| \right] \leq \mathbb{E}_{\pi_{\mathbf{y}}} \left[ \sqrt{2} \mathcal{D}_{\text{H}}(\pi_{\mathbf{x}|\mathbf{y}}, p_{\mathbf{x}|\mathbf{y}}) \left( \|\hat{h}\|_{L^2_{\pi_{\mathbf{x}|\mathbf{y}}}} + \|\hat{h}\|_{L^2_{p_{\mathbf{x}|\mathbf{y}}}} \right) \right].$$

The result then follows from (3.22), Lemma 3.5, and Hölder's inequality.  $\square$

Now we are ready to prove the main result of this section, which is a probabilistic bound for the error induced by the use of a transport map-based approximation to the D-optimality criterion.

**Theorem 3.8.** *Let  $\pi_{\mathbf{e},\mathbf{d},\mathbf{m}}$  be the joint density for the design ( $\mathbf{e}$ ), observable ( $\mathbf{d}$ ), and inference parameter ( $\mathbf{m}$ ), as defined in Section 3.1. Let  $p_{\mathbf{e},\mathbf{d},\mathbf{m}}$  be some approximation to  $\pi_{\mathbf{e},\mathbf{d},\mathbf{m}}$  satisfying  $\mathcal{D}_H(\pi_{\mathbf{e},\mathbf{d},\mathbf{m}}, p_{\mathbf{e},\mathbf{d},\mathbf{m}}) \leq \varepsilon$  for some  $\varepsilon \geq 0$ . Furthermore, for all  $\mathbf{e} \in \mathcal{E}$  and  $\mathbf{d} \in \mathcal{D}$  (with the design and observable spaces,  $\mathcal{E}$  and  $\mathcal{D}$ , defined as in Section 2), assume*

$$(3.24) \quad \sup_{\mathbf{m} \in \mathcal{M}} \frac{\pi_{\mathbf{m}|\mathbf{e},\mathbf{d}}(\mathbf{m})}{p_{\mathbf{m}|\mathbf{e},\mathbf{d}}(\mathbf{m})} \leq c_1(\mathbf{e}, \mathbf{d}) \quad \text{for all } (\mathbf{e}, \mathbf{d}) \in \mathcal{E} \times \mathcal{D} \text{ and}$$

$$(3.25) \quad \sup_{(\mathbf{d}, \mathbf{m}) \in \mathcal{D} \times \mathcal{M}} \left| \log \left( \frac{p_{\mathbf{m}|\mathbf{e},\mathbf{d}}(\mathbf{m})}{\pi_{\mathbf{m}}(\mathbf{m})} \right) \right| \leq c_2(\mathbf{e}) \quad \text{for all } \mathbf{e} \in \mathcal{E}$$

for some  $c_1 \in L^2_{\pi_{\mathbf{e},\mathbf{d}}}(\mathcal{E} \times \mathcal{D})$  and  $c_2 \in L^2_{\pi_{\mathbf{e}}}(\mathcal{E})$ . Then,

$$(3.26) \quad \mathbb{E}_{\pi_{\mathbf{e}}} \left[ \left| \Psi_D(\mathbf{e}) - \widehat{\Psi}_D(\mathbf{e}) \right| \right] \leq 4\sqrt{2}\varepsilon \left( \|c_1\|_{L^2_{\pi_{\mathbf{e},\mathbf{d}}}} + \|\hat{c}_2\|_{L^2_{\pi_{\mathbf{e}}}} \right).$$

Additionally, for any  $\zeta > 0$ ,

$$(3.27) \quad \mathbb{P}_{\pi_{\mathbf{e}}} \left[ \left| \Psi_D(\mathbf{e}) - \widehat{\Psi}_D(\mathbf{e}) \right| \leq \zeta \right] \geq 1 - \frac{4\sqrt{2}\varepsilon}{\zeta} \left( \|c_1\|_{L^2_{\pi_{\mathbf{e},\mathbf{d}}}} + \|\hat{c}_2\|_{L^2_{\pi_{\mathbf{e}}}} \right).$$

*Proof.* Let  $h(\mathbf{e}, \mathbf{d}, \mathbf{m}) := \log \left( \frac{\pi_{\mathbf{m}|\mathbf{e},\mathbf{d}}}{\pi_{\mathbf{m}}} \right)$  and  $\widehat{h}(\mathbf{e}, \mathbf{d}, \mathbf{m}) := \log \left( \frac{p_{\mathbf{m}|\mathbf{e},\mathbf{d}}}{\pi_{\mathbf{m}}} \right)$ . By the triangle inequality, we have:

$$\begin{aligned} & \mathbb{E}_{\pi_{\mathbf{e}}} \left[ \left| \Psi_D(\mathbf{e}) - \widehat{\Psi}_D(\mathbf{e}) \right| \right] \\ &= \mathbb{E}_{\pi_{\mathbf{e}}} \left[ \left| \mathbb{E}_{\pi_{\mathbf{d},\mathbf{m}|\mathbf{e}}} [h] - \mathbb{E}_{p_{\mathbf{d},\mathbf{m}|\mathbf{e}}} [\widehat{h}] \right| \right] \\ &\leq \mathbb{E}_{\pi_{\mathbf{e}}} \left[ \left| \mathbb{E}_{\pi_{\mathbf{d},\mathbf{m}|\mathbf{e}}} [h - \widehat{h}] \right| \right] + \mathbb{E}_{\pi_{\mathbf{e}}} \left[ \left| \mathbb{E}_{\pi_{\mathbf{d},\mathbf{m}|\mathbf{e}}} [\widehat{h}] - \mathbb{E}_{p_{\mathbf{d},\mathbf{m}|\mathbf{e}}} [\widehat{h}] \right| \right] \\ &= \mathbb{E}_{\pi_{\mathbf{e},\mathbf{d},\mathbf{m}}} \left[ \log \left( \frac{\pi_{\mathbf{m}|\mathbf{e},\mathbf{d}}}{p_{\mathbf{m}|\mathbf{e},\mathbf{d}}} \right) \right] + \mathbb{E}_{\pi_{\mathbf{e}}} \left[ \left| \mathbb{E}_{\pi_{\mathbf{d},\mathbf{m}|\mathbf{e}}} [\widehat{h}] - \mathbb{E}_{p_{\mathbf{d},\mathbf{m}|\mathbf{e}}} [\widehat{h}] \right| \right]. \end{aligned}$$

The first inequality (3.26) thus follows from Proposition 3.6 (with the choices  $\mathbf{x} = \mathbf{m}$  and  $\mathbf{y} = (\mathbf{e}, \mathbf{d})$ ) and Proposition 3.7 (with the choices  $\mathbf{x} = (\mathbf{d}, \mathbf{m})$ ,  $\mathbf{y} = \mathbf{e}$ , and  $\widehat{h}(\mathbf{y}, \mathbf{x}) := \widehat{h}(\mathbf{e}, \mathbf{d}, \mathbf{m}) = \log \left( \frac{p_{\mathbf{m}|\mathbf{e},\mathbf{d}}}{\pi_{\mathbf{m}}} \right)$ ). The last statement (3.27) can be deduced by applying Markov's inequality.  $\square$

**Remark 3.9** (On the assumptions of Theorem 3.8 and their consequences). *The assumption that the ratio of the posterior density  $\pi_{\mathbf{m}|\mathbf{e},\mathbf{d}}$  and its DIRT-based approximation  $p_{\mathbf{m}|\mathbf{e},\mathbf{d}}$  is bounded from above is satisfied by construction. The DIRT software [18] used in obtaining the numerical results in Section 5 constructs a “defensive” approximation to the joint density, i. e.,  $p_{\mathbf{e},\mathbf{d},\mathbf{m}} \propto \mathcal{G}_{\mathbf{e},\mathbf{d},\mathbf{m}}^2 + \tau p_{\mathbf{e},\mathbf{d},\mathbf{m}}$  for a sufficiently small constant  $\tau > 0$ . This ensures  $p_{\mathbf{e},\mathbf{d},\mathbf{m}}$  and hence  $p_{\mathbf{m}|\mathbf{e},\mathbf{d}}$  is strictly positive, thus assumption (3.24) holds.*

*The more stringent and questionable assumption is (3.25). Since  $p_{\mathbf{m}|\mathbf{e},\mathbf{d}} > 0$  by design, if  $\pi_{\mathbf{m}}(\mathbf{m}) = 0$  for some  $\mathbf{m} \in \mathcal{M}$ , the assumption is clearly violated. In practice, however, our integration domain is restricted to some bounded box that is strictly contained in the support of the prior density  $\pi_{\mathbf{m}}$ . Thus, as long as the box and prior are chosen such that  $\pi_{\mathbf{m}}$  is bounded away from zero in the restricted domain, the assumption holds, at least for Gaussian or uniform priors.*

*However, the bound  $c_2(\mathbf{e})$  from (3.25) can get arbitrarily large as the number of experiments increases. In practice, we find the approximation errors to be reasonable (and proportional to  $\mathcal{D}_H(\pi_{\mathbf{e},\mathbf{d},\mathbf{m}}, p_{\mathbf{e},\mathbf{d},\mathbf{m}})$ ) when the dimensions of  $\mathbf{e}$  and  $\mathbf{d}$  are not large, e. g., when choosing a small number of experiments to perform in the batch OED setting, or in the sequential OED setting. We also emphasize that these error bounds are not exclusive to estimators built using the DIRT procedure we outlined; they are inherent to any approximation of the D-optimality criterion using a surrogate to the density.*

*Additionally, note that for better readability, we make use of the constants  $c_1(\mathbf{e}, \mathbf{d})$  and  $c_2(\mathbf{e})$  to bound the expectations of  $\frac{\pi_{\mathbf{m}|\mathbf{e},\mathbf{d}}}{p_{\mathbf{m}|\mathbf{e},\mathbf{d}}}$  and  $\log \left( \frac{p_{\mathbf{m}|\mathbf{e},\mathbf{d}}}{\pi_{\mathbf{m}}} \right)$  respectively. Tighter upper bounds can be obtained by foregoing this simplification.*

#### 4. SEQUENTIAL OPTIMAL EXPERIMENTAL DESIGN USING CONDITIONAL DIRT

For certain applications, e. g. medical imaging or weather prediction, data is accumulated in a sequential fashion. With each incoming data set, the posterior distribution is updated to account for the knowledge gained from the new observations. These settings lend themselves naturally to *adaptive* or *sequential* optimal design (SOED). In SOED, experimental conditions or designs are chosen in stages to optimize an *incremental* utility function that incorporates the current state of knowledge (i. e., posterior) about the unknown parameters. In [Section 4.1](#) we describe a greedy approach to solving the SOED problem and identify the main challenges in finding optimal sequential designs. The transport map approach for OED described in [Section 3.3](#) is extended to sequential OED in [Section 4.2](#). [Section 4.3](#) discusses how to incorporate existing transport maps into preconditioners facilitating more efficient approximations to the SOED objective functions.

**4.1. A Greedy Approach to Sequential Optimal Experimental Design.** While the OED formulation described in the preceding sections is used for finding designs given only the prior information, in SOED the posterior is iteratively updated and designs are chosen adaptively in distinct stages. As is the case in standard OED, optimality is defined in terms of the level of uncertainty in the posterior distribution. However, the key difference between OED and SOED is the inclusion of a feedback loop into the optimization problem, as visualized in [Figure 4.1](#).

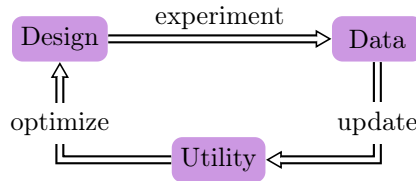


FIGURE 4.1. Flowchart of SOED procedure depicting iteration between finding optimal designs, using them to conduct the experiment and collect data, and updating the state of knowledge and utility function using the newly-collected data.

For a fixed budget of  $K \in \mathbb{N}$  experiments, the solution to the SOED problem is a set of design *functions* (or policies)  $\{e_k^*(\pi_{\mathbf{m}}^{k-1})\}_{k=0}^{K-1}$  that depend on the current state of knowledge about  $\mathbf{m}$ , which is defined by the posterior density  $\{\pi_{\mathbf{m}}^k\}_{k=-1}^{K-2}$ . Finding the optimal set of design functions requires solving a dynamic programming problem as described in [31, Chapter 3]. However, the numerical solution of the dynamic programming problem is extremely costly since it involves nested optimization and suffers from the curse of dimensionality.

Thus, we employ a greedy approach to solving the SOED problem. Unlike the dynamic programming formulation, the greedy formulation of SOED is myopic, hence the curse of dimensionality is avoided. Due to this simplification, the sequential designs  $\{e_k^*\}_{k=0}^{K-1}$  obtained using the greedy optimization approach will generally be *sub-optimal* for a fixed number of experiments  $K$ . However, the approach does have advantages in the absence of a hard limit on the number of experiments that can be performed. Additional experiments can be included seamlessly using the greedy approach, whereas the number of experiments must be chosen a priori in the dynamic programming context.

To facilitate the discussion, we define a recursive formula for updating the state of knowledge, or posterior density, in between experimental stages:

$$(4.1) \quad \pi_{\mathbf{m}}^k := \pi_{\mathbf{m}|e_k, \mathbf{d}_k, \mathbf{I}_{k-1}} = \frac{\pi_{\mathbf{d}_k|\mathbf{m}, e_k, \mathbf{I}_{k-1}} \cdot \pi_{\mathbf{m}}^{k-1}}{\pi_{\mathbf{d}_k|e_k, \mathbf{I}_{k-1}}} = \frac{\pi_{\mathbf{d}_k|\mathbf{m}, e_k, \mathbf{I}_{k-1}} \cdot \pi_{\mathbf{m}|\mathbf{I}_{k-1}}}{\pi_{\mathbf{d}_k|e_k, \mathbf{I}_{k-1}}},$$

for  $k = 0, \dots, K-1$ , where  $\mathbf{I}_{k-1} := \{(e_i^*, \mathbf{d}_i^*)\}_{i=1}^{k-1}$  stores the history of optimal designs and their corresponding observations up until stage  $k-1$ . We define  $\pi_{\mathbf{m}}^{-1} := \pi_{\mathbf{m}}$ , and  $\mathbf{I}_{-1}$  to be the empty set,  $\mathbf{I}_{-1} := \emptyset$ . In deriving the last equality we have assumed that the stage  $k-1$  posterior is independent of the decision to be made at the next stage, i. e.,  $\pi_{\mathbf{m}|e_k, \mathbf{I}_{k-1}} = \pi_{\mathbf{m}|\mathbf{I}_{k-1}}$ .

In the greedy approach to SOED, given the current state of knowledge, the  $k$ -th design vector  $\mathbf{e}_k^*$  is chosen to optimize the stage  $k$  reward,

$$(4.2) \quad \Psi^k(\mathbf{e}_k, \pi_{\mathbf{m}}^{k-1}) = \mathbb{E}_{\pi_{\mathbf{d}_k | \mathbf{e}_k, \mathbf{I}_{k-1}}} [\psi^k(\mathbf{e}_k, \mathbf{d}_k, \pi_{\mathbf{m}}^{k-1})],$$

which is an expectation of a stage  $k$  utility function  $\psi^k$ . As before, the SOED utility function is problem-specific and there are analogues of the A- and D-optimality criteria defined for OED in (2.5) and (2.6).

For the remainder of this section, we target our discussion to the D-optimality SOED utility function,  $\psi_D^k$ , which is defined as

$$(4.3) \quad \begin{aligned} \psi_D^k(\mathbf{e}_k, \mathbf{d}_k, \pi_{\mathbf{m}}^{k-1}) &= \mathcal{D}_{\text{KL}}(\pi_{\mathbf{m} | \mathbf{e}_k, \mathbf{d}_k, \mathbf{I}_{k-1}} \| \pi_{\mathbf{m}}^{k-1}) \\ &= \mathcal{D}_{\text{KL}}(\pi_{\mathbf{m} | \mathbf{e}_k, \mathbf{d}_k, \mathbf{I}_{k-1}} \| \pi_{\mathbf{m} | \mathbf{I}_{k-1}}) \end{aligned}$$

for  $k = 0, \dots, K-1$ . The D-optimal greedy sequential designs are obtained by maximizing the *incremental* expected information gain in each stage of the procedure. For generality, we allow the design and observation spaces to vary between stages and denote the stage-dependent spaces by  $\mathcal{E}_k$  and  $\mathcal{D}_k$  respectively. The general approach for finding greedy sequential designs using the EIG criteria is summarized as follows:

- (1) Initialize  $\pi_{\mathbf{m}}^{-1} = \pi_{\mathbf{m}}$ ,  $\mathbf{I}_{-1} = \emptyset$ , and  $k = 0$ .
- (2) At stage  $k$ , find an optimal  $k$ -th design vector  $\mathbf{e}_k^*$  that maximizes
 
$$\Psi_D^k(\mathbf{e}_k, \pi_{\mathbf{m}}^{k-1}) = \mathbb{E}_{\pi_{\mathbf{d}_k | \mathbf{e}_k, \mathbf{I}_{k-1}}} [\psi_D^k(\mathbf{e}_k, \mathbf{d}_k, \pi_{\mathbf{m}}^{k-1})]$$
 over  $\mathbf{e}_k \in \mathcal{E}_k$ .
- (3) Perform experiment  $k$  with design vector  $\mathbf{e}_k^*$  to obtain data  $\mathbf{d}_k^* \in \mathcal{D}$ .
- (4) Update  $\mathbf{I}_k = \{\mathbf{I}_{k-1}, \mathbf{e}_k^*, \mathbf{d}_k^*\}$  and  $\pi_{\mathbf{m}}^k = \pi_{\mathbf{m} | \mathbf{I}_k}$ .
- (5) Increment  $k$  and repeat steps (2) to (4) until all experiments have been performed or sufficient reduction in posterior uncertainty has been achieved.

In the following section we focus on step (2) and extend the KR-based approach of Section 3 to numerically approximate the incremental expected information gain  $\Psi_D^k$ .

**4.2. Knothe-Rosenblatt-Based Approximation to the Incremental Expected Information Gain.** Assume we are given the fixed history sequence  $\mathbf{I}_{k-1}$  as well as a KR transport map  $\mathcal{T}^{k-1}$  coupling an approximation of  $\pi_{\mathbf{e}_{k-1}, \mathbf{d}_{k-1}, \mathbf{m} | \mathbf{I}_{k-2}}$  to the reference density  $\rho_{\mathbf{e}, \mathbf{d}, \mathbf{m}}$ . At the beginning of the  $k$ -th experimental stage, a KR map surrogate is built to approximate the  $k$ -th joint conditional density, which in the most general form satisfies

$$(4.4) \quad \pi_{\mathbf{e}_k, \mathbf{d}_k, \mathbf{m} | \mathbf{I}_{k-1}} = \pi_{\mathbf{d}_k | \mathbf{e}_k, \mathbf{m}, \mathbf{I}_{k-1}} \cdot \pi_{\mathbf{m} | \mathbf{I}_{k-1}} \cdot \pi_{\mathbf{e}_k | \mathbf{I}_{k-1}}.$$

The  $k$ -th incremental likelihood  $\pi_{\mathbf{d}_k | \mathbf{e}_k, \mathbf{m}, \mathbf{I}_{k-1}}$  and design density  $\pi_{\mathbf{e}_k | \mathbf{I}_{k-1}}$  are both user-specified through the model (see Remark 4.1), and the stage  $k-1$  posterior  $\pi_{\mathbf{m} | \mathbf{I}_{k-1}}$  can be approximated using  $\mathcal{T}^{k-1}$ . Thus, the transport map  $\mathcal{T}^k$  can be built in a recursive fashion using the DIRT Algorithm 1 to satisfy

$$(4.5) \quad (\mathcal{T}^k)_\# \rho_{\mathbf{e}, \mathbf{d}, \mathbf{m}} \approx \pi_{\mathbf{d}_k | \mathbf{e}_k, \mathbf{m}, \mathbf{I}_{k-1}} \cdot \pi_{\mathbf{e}_k | \mathbf{I}_{k-1}} \cdot p_{\mathbf{m} | \mathbf{I}_{k-1}} \approx \pi_{\mathbf{e}_k, \mathbf{d}_k, \mathbf{m} | \mathbf{I}_{k-1}}$$

where  $p_{\mathbf{m} | \mathbf{I}_{k-1}} = (\mathcal{T}_{\mathbf{m} | \mathbf{e}_{k-1}^*, \mathbf{d}_{k-1}^*}^{k-1})_\# \rho_{\mathbf{m}}$  with  $\mathcal{T}_{\mathbf{m} | \mathbf{e}_{k-1}^*, \mathbf{d}_{k-1}^*}^{k-1}$  defined analogously to (3.3). Once this map is constructed, the incremental expected information gain  $\Psi_D^k(\mathbf{e}_k, \pi_{k-1})$  can be approximated at any  $\mathbf{e}_k \in \mathcal{E}_k$  using Algorithm 3,

$$(4.6) \quad \Psi_D^k(\mathbf{e}_k, \pi_{k-1}) \approx \widehat{\Psi}_D^k(\mathbf{e}_k, p_{\mathbf{m} | \mathbf{I}_{k-1}}) := \text{D}_{\text{OPT}}(\rho_{\mathbf{e}, \mathbf{d}, \mathbf{m}}, \mathcal{T}^k, p_{\mathbf{m} | \mathbf{I}_{k-1}}, \mathbf{e}_k, N).$$

While this approach is straightforward to iterate, it suffers from two major drawbacks. First of all, there is a sequential accumulation of error due to the recursive use of the KR maps to approximate  $\pi_{\mathbf{m} | \mathbf{I}_{k-1}}$  in the  $k$ -th joint density. Even if  $\mathcal{T}^{k-1}$  is built to ensure  $\mathcal{D}_{\text{H}}(\pi_{\mathbf{e}_{k-1}, \mathbf{d}_{k-1}, \mathbf{m} | \mathbf{I}_{k-2}}, \mathcal{T}_\#^{k-1} \rho_{\mathbf{e}, \mathbf{d}, \mathbf{m}}) \leq \varepsilon$  for sufficiently small  $\varepsilon \ll 1$ , a small  $\mathcal{D}_{\text{H}}(\pi_{\mathbf{m} | \mathbf{e}_{k-1}^*, \mathbf{d}_{k-1}^*, \mathbf{I}_{k-2}}, (\mathcal{T}_{\mathbf{m} | \mathbf{e}_{k-1}^*, \mathbf{d}_{k-1}^*}^{k-1})_\# \rho_{\mathbf{m}})$  for any  $\mathbf{e}_k^*, \mathbf{d}_k^*$  can only be ensured with some probability (see Proposition 3.2). Thus there is a chance that  $p_{\mathbf{m} | \mathbf{I}_{k-1}}$  is not a sufficient approximation to  $\pi_{\mathbf{m} | \mathbf{I}_{k-1}}$ . The second major flaw of this approach is that it does not fully exploit all the information learned up until the current stage, e.g. about the correlation structures and

regions of concentration. Thus, in this naive approach, computational resources are wasted to relearn information. Both these challenges are addressed in [Section 4.3](#).

**Remark 4.1** (Incremental likelihood and density). *The exact forms of the incremental likelihood  $\pi_{\mathbf{d}_k | \mathbf{e}_k, \mathbf{m}, \mathbf{I}_{k-1}}$  and  $k$ -th design density  $\pi_{\mathbf{e}_k | \mathbf{I}_{k-1}}$  are model-dependent. For example, if one couples the  $k$ -th observations  $\mathbf{d}_k \in \mathcal{D}_k$ ,  $k$ -th design  $\mathbf{e}_k \in \mathcal{E}_k$ , and inference parameters  $\mathbf{m}$  via*

$$(4.7) \quad \mathbf{d}_k = \mathcal{F}(\mathbf{e}_k, \mathbf{m}) + \boldsymbol{\eta}_k, \quad \boldsymbol{\eta}_k \sim \mathcal{N}(0, \sigma_k^2 \text{id}),$$

and assumes the only explicit dependence on the history vector  $\mathbf{I}_{k-1}$  is through the stage  $k$  prior  $\mathbf{m} \sim \pi_{\mathbf{m} | \mathbf{I}_{k-1}}$ , then the stage  $k$  likelihood is independent of  $\mathbf{I}_{k-1}$  and satisfies

$$(4.8) \quad \pi_{\mathbf{d}_k | \mathbf{e}_k, \mathbf{m}} \propto \exp \left[ -\frac{1}{2\sigma_k^2} \|\mathcal{F}(\mathbf{e}_k, \mathbf{m}) - \mathbf{d}_k\|^2 \right].$$

Likewise, the design density is independent of  $\mathbf{I}_{k-1}$ , i. e.,  $\pi_{\mathbf{e}_k | \mathbf{I}_{k-1}} = \pi_{\mathbf{e}_k}$ . This is the form of the  $k$ -th likelihood used in [Section 5](#).

**4.3. Preconditioned Knothe-Rosenblatt maps for SOED.** To alleviate the latter drawback of the straightforward approach, we propose a preconditioning method that enables incorporation of previously acquired knowledge. This approach helps reduce the number of layers required in the sequential construction of the DIRT maps  $\{\mathcal{T}^k\}_{k=0}^{K-1}$  and the amount of unnormalized density evaluations needed for constructing the FTT decomposition. The idea driving the preconditioning approach is similar to the reasoning behind the layered construction of the deep inverse Rosenblatt transports.

To outline the idea, assume  $\widehat{p}_{\mathbf{e}, \mathbf{d}, \mathbf{m}}^k$  is a probability density that captures (some of) the complex nonlinear interactions present in the  $k$ -th joint target density  $\pi_{\mathbf{e}_k, \mathbf{d}_k, \mathbf{m} | \mathbf{I}_{k-1}}$ . Let  $\mathcal{L}^k: \mathbb{R}^n \rightarrow \mathbb{R}^n$  be a lower-triangular order-preserving transport map satisfying  $(\mathcal{L}^k)_\# \rho_{\mathbf{e}, \mathbf{d}, \mathbf{m}} = \widehat{p}_{\mathbf{e}, \mathbf{d}, \mathbf{m}}^k$ . Then  $\mathcal{L}^k$  can be used to precondition  $\pi_{\mathbf{e}_k, \mathbf{d}_k, \mathbf{m} | \mathbf{I}_{k-1}}$  and reduce the computational cost of the tensor train-based construction of  $\mathcal{T}^k$ . Rather than approximating the joint density directly, a KR map  $\mathcal{K}^k$  is constructed to approximate  $q_k$ , where

$$(4.9) \quad q_k = (\mathcal{L}^k)_\# \pi_{\mathbf{e}_k, \mathbf{d}_k, \mathbf{m} | \mathbf{I}_{k-1}}.$$

The map  $\mathcal{T}^k$  is then defined as the composition  $\mathcal{T}^k = \mathcal{L}^k \circ \mathcal{K}^k$ , and is lower-triangular and order-preserving by construction. This can be viewed as a sequential change-of-variables

$$\mathbf{v} \xrightarrow{\mathcal{K}^k} \mathbf{z}_k \xrightarrow{\mathcal{L}^k} \mathbf{x}_k,$$

where,  $\mathbf{v} \sim \rho_{\mathbf{e}, \mathbf{d}, \mathbf{m}}$ ,  $\mathbf{z}_k \sim \widehat{q}_k \approx q_k$  and  $\mathbf{x}_k \sim p_{\mathbf{e}_k, \mathbf{d}_k, \mathbf{m} | \mathbf{I}_{k-1}} \approx \pi_{\mathbf{e}_k, \mathbf{d}_k, \mathbf{m} | \mathbf{I}_{k-1}}$ .

The preconditioning maps  $\{\mathcal{L}^k\}_{k=1}^{K-1}$  can be defined in various ways, and the “best” choice is generally problem-specific. Here, we outline the preconditioning approach used for the computations in [Section 5](#). In this approach, a running KR-based approximation  $p_{\mathbf{m}}^k \approx \pi_{\mathbf{m} | \mathbf{I}_k} =: \pi_{\mathbf{m}}^k$  (for  $k = 0, \dots, K-2$ ) is kept and updated after each experiment is performed. Denoting the KR map that pushes  $\rho_{\mathbf{m}}$  forward to  $p_{\mathbf{m}}^k$  with  $\mathcal{T}_{\mathbf{m}}^k: \mathbb{R}^{n_m} \rightarrow \mathbb{R}^{n_m}$ , for  $k = 1, \dots, K-1$  we define the augmented diagonal preconditioner as

$$(4.10) \quad \mathcal{L}^k(\mathbf{z}_k) := \mathcal{L}^k(\mathbf{z}_{e_k}, \mathbf{z}_{d_k}, \mathbf{z}_m) = \begin{bmatrix} \mathcal{R}_{\mathbf{e}}^k(\mathbf{z}_{e_k}) \\ \text{id}_{\mathbf{d}}(\mathbf{z}_{d_k}) \\ \mathcal{T}_{\mathbf{m}}^k(\mathbf{z}_m) \end{bmatrix}$$

where  $\mathbf{z}_{e_k} \in \mathbb{R}^{n_e}$ ,  $\mathbf{z}_{d_k} \in \mathcal{D} \subset \mathbb{R}^{n_d}$ ,  $\mathbf{z}_m \in \mathbb{R}^{n_m}$  and  $\mathcal{R}_{\mathbf{e}}^k$  denotes the KR rearrangement such that  $(\mathcal{R}_{\mathbf{e}}^k)_\# \rho_{\mathbf{e}}(\mathbf{e}_k) = \pi_{\mathbf{e}_k | \mathbf{I}_{k-1}}(\mathbf{e}_k)$ . If  $\mathcal{R}_{\mathbf{e}}^k$  is not known, it could be replaced by the identity operator  $\text{id}_{\mathbf{e}}$ .

In contrast to [\(4.5\)](#), the more accurate posterior surrogate  $p_{\mathbf{m}}^k$  is used to approximate the stage  $k+1$  joint density,

$$(4.11) \quad \pi_{\mathbf{e}_{k+1}, \mathbf{d}_{k+1}, \mathbf{m} | \mathbf{I}_k} \approx \pi_{\mathbf{d}_{k+1} | \mathbf{e}_{k+1}, \mathbf{m}, \mathbf{I}_k} \cdot \pi_{\mathbf{e}_{k+1} | \mathbf{I}_k} \cdot p_{\mathbf{m}}^k.$$

Using the preconditioner [\(4.10\)](#), the specific form of the  $k$ -th preconditioned density [\(4.9\)](#) to be approximated is

$$q_k(\mathbf{z}_e, \mathbf{z}_d, \mathbf{z}_m) = \pi_{\mathbf{d}_k | \mathbf{e}_k, \mathbf{m}, \mathbf{I}_{k-1}}(\mathbf{z}_{d_k} | \mathcal{R}^k(\mathbf{z}_{e_k}), \mathcal{T}_{\mathbf{m}}^k(\mathbf{z}_m)) \rho_{\mathbf{e}}(\mathbf{z}_{e_k}) \rho_{\mathbf{m}}(\mathbf{z}_m),$$

and all the computational difficulties in building the KR map stem from the incremental likelihood.

To limit the number of posterior density evaluations (and hence the number of applications of the parameter-to-observable map  $\mathcal{F}$ ), the running approximations to the posterior densities are constructed in a recursive fashion using a DIRT procedure guided by the sequence of bridging densities  $\{\pi_{\mathbf{m}}^k\}_{k=0}^{K-2}$ . The output of this DIRT-based algorithm is a sequence of transport maps  $\{\mathcal{T}_{\mathbf{m}}^k\}_{k=0}^{K-2}$  satisfying  $(\mathcal{T}_{\mathbf{m}}^k)_{\#} \rho_{\mathbf{m}} = p_{\mathbf{m}}^k \approx \pi_{\mathbf{m}}^k$ . As mentioned towards the end of Section 3.2, these bridging densities are a natural choice for posteriors stemming from Bayesian inverse problems with large amounts of data, or for sequential Bayesian inference. Since these bridging densities allow the information to trickle in experiment by experiment, the densities  $\{\pi_{\mathbf{m}}^k\}_{k=0}^{K-2}$  exhibit a sequential concentration to the most likely subregion of  $\mathcal{M}$ .

**Remark 4.2** (DIRT map approximation to the posterior densities). *Since the sequence of posterior densities  $\{\pi_{\mathbf{m}|I_k}\}_{k=0}^{K-2}$  are obtained by performing experiments with conditions that maximize the incremental expected information gain  $\mathcal{D}_{\text{KL}}(\pi_{\mathbf{m}|e_{k+1}, \mathbf{d}_{k+1}, I_k} \| \pi_{\mathbf{m}|I_k})$ , the Hellinger distance between adjacent posteriors may be too large to guarantee sufficient accuracy of the corresponding composite transport map built using the DIRT procedure. Thus for certain problems it is necessary to combine the tempering approach discussed in Section 3.2 with the sequential data accumulation approach discussed in Section 4.3 to obtain a composite set of bridging densities.*

Specifically, given a transport map satisfying  $(\mathcal{T}_{\mathbf{m}}^{k-1})_{\#} \rho_{\mathbf{m}} = \pi_{\mathbf{m}|I_{k-1}}$ , the next stage transport map  $\mathcal{T}_{\mathbf{m}}^k$  coupling  $\rho_{\mathbf{m}}$  and  $\pi_{\mathbf{m}|I_k}$  is constructed recursively,  $\mathcal{T}_{\mathbf{m}}^k = \mathcal{T}_{\mathbf{m}}^{k-1} \circ \mathcal{K}_{\mathbf{m}}^k$ . The map  $\mathcal{K}_{\mathbf{m}}^k$  ensures  $(\mathcal{K}_{\mathbf{m}}^k)_{\#} \rho_{\mathbf{m}} \approx (\mathcal{T}_{\mathbf{m}}^{k-1})_{\#} \pi_{\mathbf{m}|I_k}$  and is constructed using the DIRT Algorithm 1 with the bridging densities  $\{\pi_{\mathbf{e}_k}^{\ell}\}_{\ell=0}^{\ell_k}$  defined as

$$(4.12) \quad \pi_{\mathbf{e}_k}^{\ell} = (\pi_{\mathbf{d}_k | e_k, \mathbf{m}})^{\beta_k^{\ell}} \rho_{\mathbf{m}}$$

with exponents  $0 < \beta_k^0 < \beta_k^1 < \dots < \beta_k^{\ell_k} = 1$ , and  $\pi_{\mathbf{e}_k}^{\ell_k} = (\mathcal{T}_{\mathbf{m}}^{k-1})_{\#} \pi_{\mathbf{m}|I_k}$ .

Due to the recursive layered approximation to the posterior density, the errors still accumulate in the sequential KR approximation (4.11) to  $\pi_{e_k, \mathbf{d}_k, \mathbf{m}|I_{k-1}}$ . However, this stems from the error accumulation in the direct approximation of the posterior density and can thus be controlled deterministically. The amount of additional applications of the PTO map required to keep the running approximation to the posterior density is generally offset by the reduction in computation offered by using the resulting preconditioning operator  $\mathcal{L}^k$  defined in (4.10). We present the full posterior-preconditioned SOED procedure used in the next section in Algorithm 5, where we again leave the optimization algorithm used to maximize the incremental EIG arbitrary. A visual representation of the algorithm in the form of a flowchart is also included in Figure 4.2.

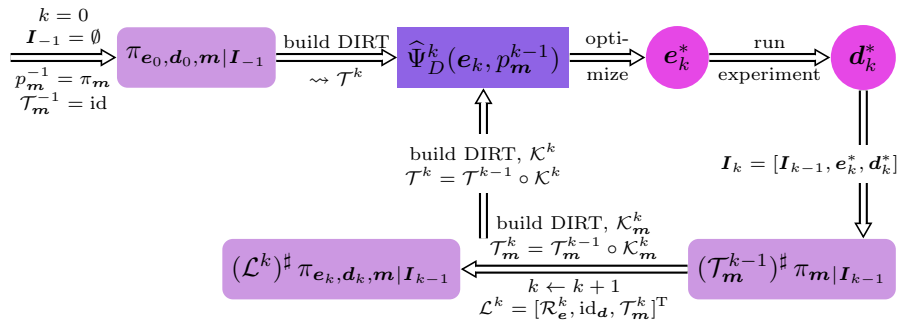


FIGURE 4.2. Flowchart visualization of the greedy preconditioned SOED procedure outlined in Algorithm 5.

## 5. NUMERICAL EXAMPLES

We demonstrate the effectiveness of our proposed method on finding optimal designs for two model problems. In Section 5.1, we consider a non-intrusive sensor placement type OED problem and use the transport-map-based procedures (Algorithm 5 and Algorithm 4) to compute optimal testing times for a

---

**Algorithm 5** Greedy posterior-preconditioned SOED using incremental EIG criterion.
 

---

```

1: procedure SOED( $K, \rho_{\mathbf{e}}, \mathbf{d}, \mathbf{m}, \pi_{\mathbf{e}_0}, \pi_{\mathbf{m}}, \pi_{\mathbf{d}_0|\mathbf{e}_0, \mathbf{m}}, \varepsilon, \epsilon$ )
2:    $\mathcal{L}^0 \leftarrow \text{id}_n, \mathcal{T}_{\mathbf{m}}^{-1} \leftarrow \text{id}_{n_{\mathbf{m}}}, p_{\mathbf{m}}^{-1} \leftarrow \pi_{\mathbf{m}}, \mathbf{I}_{-1} = \emptyset$  # initialization
3:   Choose initial bridging densities  $\{\pi_{\mathbf{e}_0, \mathbf{d}_0, \mathbf{m}}^\ell\}_{\ell=0}^{k_0}$ 
4:   for  $k = 0, \dots, K-1$  do
5:      $\pi_{\mathbf{e}_k, \mathbf{d}_k, \mathbf{m}|\mathbf{I}_{k-1}} \leftarrow \pi_{\mathbf{d}_k|\mathbf{e}_k, \mathbf{m}, \mathbf{I}_{k-1}} \cdot p_{\mathbf{m}}^{k-1} \cdot \pi_{\mathbf{e}_k|\mathbf{I}_{k-1}}$ 
6:      $q_k \leftarrow (\mathcal{L}^k)^\sharp \pi_{\mathbf{e}_k, \mathbf{d}_k, \mathbf{m}|\mathbf{I}_{k-1}}$ 
7:     Choose bridging densities  $\{q_k^\ell\}_{\ell=0}^{k_k}$ 
8:      $\mathcal{K}^k \leftarrow \text{DIRT}(\rho_{\mathbf{e}}, \mathbf{d}, \mathbf{m}, \{q_k^\ell\}_{\ell=0}^{k_k}, \varepsilon)$ 
9:      $\mathcal{T}^k \leftarrow \mathcal{L}^k \circ \mathcal{K}^k$ 
10:    Choose  $\mathbf{e}_k^* \in \text{Arg max}_{\mathbf{e}_k \in \mathcal{E}} \text{DOpt}(\rho_{\mathbf{e}}, \mathbf{d}, \mathbf{m}, \mathcal{T}^k, p_{\mathbf{m}}^{k-1}, \mathbf{e}_k)$ 
11:    Perform experiment with  $\mathbf{e}_k^*$  and acquire  $\mathbf{d}_k^*$ 
12:     $\mathbf{I}_k = \{\mathbf{I}_{k-1}, \mathbf{e}_k^*, \mathbf{d}_k^*\}$ 
13:    Choose bridging densities  $\{\pi_k^\ell\}_{\ell=0}^{\ell_k}$  for  $(\mathcal{T}_{\mathbf{m}}^{k-1})^\sharp \pi_{\mathbf{m}|\mathbf{I}_k}$  as in Remark 4.2
14:     $\mathcal{K}_{\mathbf{m}}^k \leftarrow \text{DIRT}(\rho_{\mathbf{m}}, \{\pi_k^\ell\}_{\ell=0}^{\ell_k}, \epsilon)$ 
15:     $\mathcal{T}_{\mathbf{m}}^k = \mathcal{T}_{\mathbf{m}}^{k-1} \circ \mathcal{K}_{\mathbf{m}}^k$ 
16:    Update  $\mathcal{L}^k$  using equation (4.10) and  $\mathcal{T}_{\mathbf{m}}^k$ 
17:  end for
18:  return  $\{\mathbf{e}_k^*\}_{k=0}^{K-1}, \{\mathbf{d}_k^*\}_{k=0}^{K-1}, \mathcal{T}_{\mathbf{m}}^{K-1}$ 
19: end procedure

```

---

disease model inverse problem. In Section 5.2 we instead consider an intrusive design, i. e., we choose optimal boundary conditions for an inverse problem with an elliptic forward operator. The algorithms used in both examples are implemented in MATLAB using the DIRT FTT codes found in the deep-tensor toolbox [18].

### 5.1. Optimal Observation Times for Parameter Inversion Using the SEIR Disease Model.

As a first example, we consider the susceptible-exposed-infected-removed (SEIR) model commonly used for describing the spread of infectious diseases. Under the assumption of constant population size, the SEIR model is comprised of the following system of ordinary differential equations,

$$(5.1) \quad \begin{aligned} \frac{dS}{dt} &= -\beta(t) S I, & \frac{dE}{dt} &= \beta(t) S I - \alpha E, \\ \frac{dI}{dt} &= \alpha E - \gamma(t) I, & \frac{dR}{dt} &= (\gamma^r + \gamma^d(t)) I, \end{aligned}$$

where the variables  $S(t), E(t), I(t), R(t)$  are used to denote the fractions of susceptible, exposed, infected and removed individuals at time  $t$ , respectively, and are initialized with  $S(0) = 99, E(0) = 1$ , and  $I(0) = R(0) = 0$ . The parameters to be estimated are  $\beta(t), \alpha, \gamma^r, \gamma^d(t)$ , where the constants  $\alpha$  and  $\gamma^r$  denote the rate of susceptibility to exposure and infection to recovery, respectively. To simulate the effect of policy changes or other time-dependent factors (e. g., quarantine and overcrowding of hospitals), the rates at which exposed individuals become infected and infected individuals perish are assumed to be time-dependent and are parametrized as follows:

$$\begin{aligned} \beta(t) &= \beta_1 + \frac{\tanh(7(t-\tau))}{2} (\beta_2 - \beta_1), \\ \gamma^d(t) &= \gamma_1^d + \frac{\tanh(7(t-\tau))}{2} (\gamma_2^d - \gamma_1^d), \end{aligned}$$

i. e., the rates transition smoothly from some initial rate ( $\beta_1$  and  $\gamma_1^d$ ) to some final rate ( $\beta_2$  and  $\gamma_2^d$ ) around time  $\tau > 0$ .

In the following, we fix  $\tau = 2.1$  and an overall time interval of  $[0, 4]$ . The time interval  $[1, 3]$  is split into 4 disjoint subintervals,  $\{(a_i, a_{i+1})\}_{i=1}^4$  (with  $a_i = 1 + 0.5(i-1)$ ) and the goal of the optimal design problem is to choose four times  $e_i \in (a_i, a_{i+1})$ , one in each interval, at which to measure the number

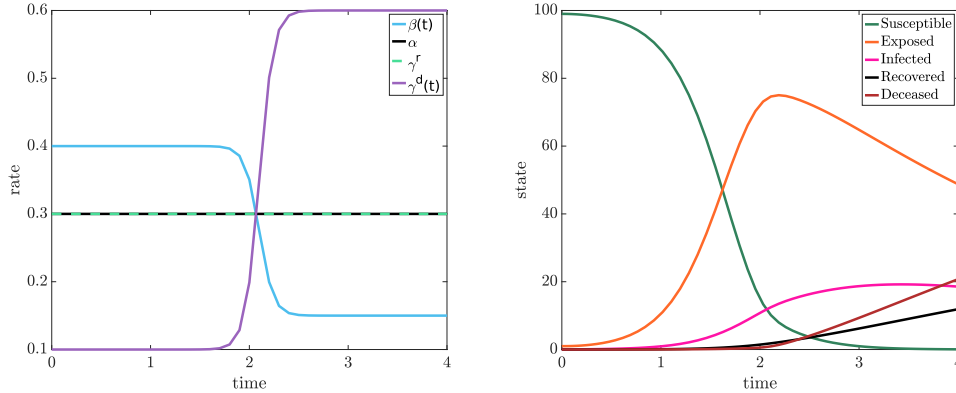


FIGURE 5.1. The true rates used for synthesizing data and the corresponding solution to the system (5.1) are visualized on the left and right, respectively.

of infected and deceased individuals for optimal inference of the 6 rates  $\mathbf{m} = [\beta_1, \alpha, \gamma^r, \gamma_1^d, \beta_2, \gamma_2^d]$ . We consider two ways to find the four optimal times  $e_1, \dots, e_4$ : (i) choosing them one at a time using a greedy sequential procedure (yielding the optimal design vector  $\mathbf{e}_{\text{SOED-1}}^*$ ), and (ii) planning two subsequent observation times simultaneously using a greedy sequential procedure (yielding the optimal design vector  $\mathbf{e}_{\text{SOED-2}}^*$ ). To set up the Bayesian inverse problem, a uniform prior on  $[0, 1]$  is assigned to each unknown rate, i. e.,  $\pi_{\mathbf{m}} = \mathbb{1}_{[0,1]^6}$ . The measurement noise at each observation time is assumed to be uncorrelated and Gaussian with zero mean and standard deviation  $\sigma_I = 2$  for the measured number of infected individuals and  $\sigma_{R^d} = 1$  for the measured number of deceased individuals.

We choose a fixed “true” parameter  $\mathbf{m}_{\text{true}} = [0.4, 0.3, 0.3, 0.1, 0.15, 0.6]^T$  in the following experiments and focus on finding designs maximizing the EIG, i. e., the D-optimality criterion. For all experiments, the dynamics are simulated in MATLAB using `ode45` to solve the system of equations (5.1) and MATLAB’s `fmincon` function is used to maximize the objective function. Simple bound constraints ensure that  $e_i$  remains inside the corresponding time interval. A visualization of the true rates as well as the corresponding solution to the SEIR model (5.1) is provided in Figure 5.1

We begin with experiment (ii). Using Algorithm 4 with  $N = 10\,000$  samples to approximate the EIG, we solve the greedy sequential design problem and plan the four optimal observation times two at a time, leading to the final optimal design vector  $\mathbf{e}_{\text{SOED-2}}^*$ . Construction of the DIRT approximation to the two joint densities for the  $4 + 2 + 6 = 12$ -dimensional random variables  $\mathbf{e}, \mathbf{d}, \mathbf{m}$  as well as the intermediate posterior density  $\pi_{\mathbf{m}|e_{1:2}, d_{1:2}}^*$  required 350 650 evaluations of the corresponding unnormalized densities, where each evaluation takes approximately  $3.5 \times 10^{-3}$  s on average.

We also find the optimal allocation of testing times in a purely sequential fashion ( $\mathbf{e}_{\text{SOED-1}}^*$ ) for a fixed set of inference parameters using Algorithm 5, i. e., experiment (i). Again,  $N = 10\,000$  samples are used to approximate the incremental EIG in each stage of the SOED procedure. The total procedure for finding four optimal observation times using the greedy sequential fashion required 147 987 solves of the SEIR ODE system.

Figure 5.2 provides a visual comparison of the posterior densities using data synthesized at the two “optimal” designs  $\mathbf{e}_{\text{SOED-1}}^*$  and  $\mathbf{e}_{\text{SOED-2}}^*$ . They are also compared to the posterior density resulting from data measured uniformly at the beginning of each time interval,  $\mathbf{e}_{\text{UNIF}} = [a_1, a_2, a_3, a_4]$ . For each design choice, the resulting posterior density was estimated using the DIRT Algorithm 1 such that  $\mathcal{D}_{\text{H}}(p_{\mathbf{m}|\mathbf{e}^*, \mathbf{d}^*}, \pi_{\mathbf{m}|\mathbf{e}^*, \mathbf{d}^*})$  is around  $10^{-2}$ . Both optimal design choices lead to more concentrated posterior densities than  $\mathbf{e}_{\text{UNIF}}$  over most of the parameters, however  $\mathbf{e}_{\text{UNIF}}$  outperforms both optimal designs in learning the infection rate  $\alpha$ . The overall superiority of  $\mathbf{e}_{\text{SOED-1}}^*$  and  $\mathbf{e}_{\text{SOED-2}}^*$  is also supported by comparing the KL divergence from posterior to prior. Using 100 000 samples to approximate the KL

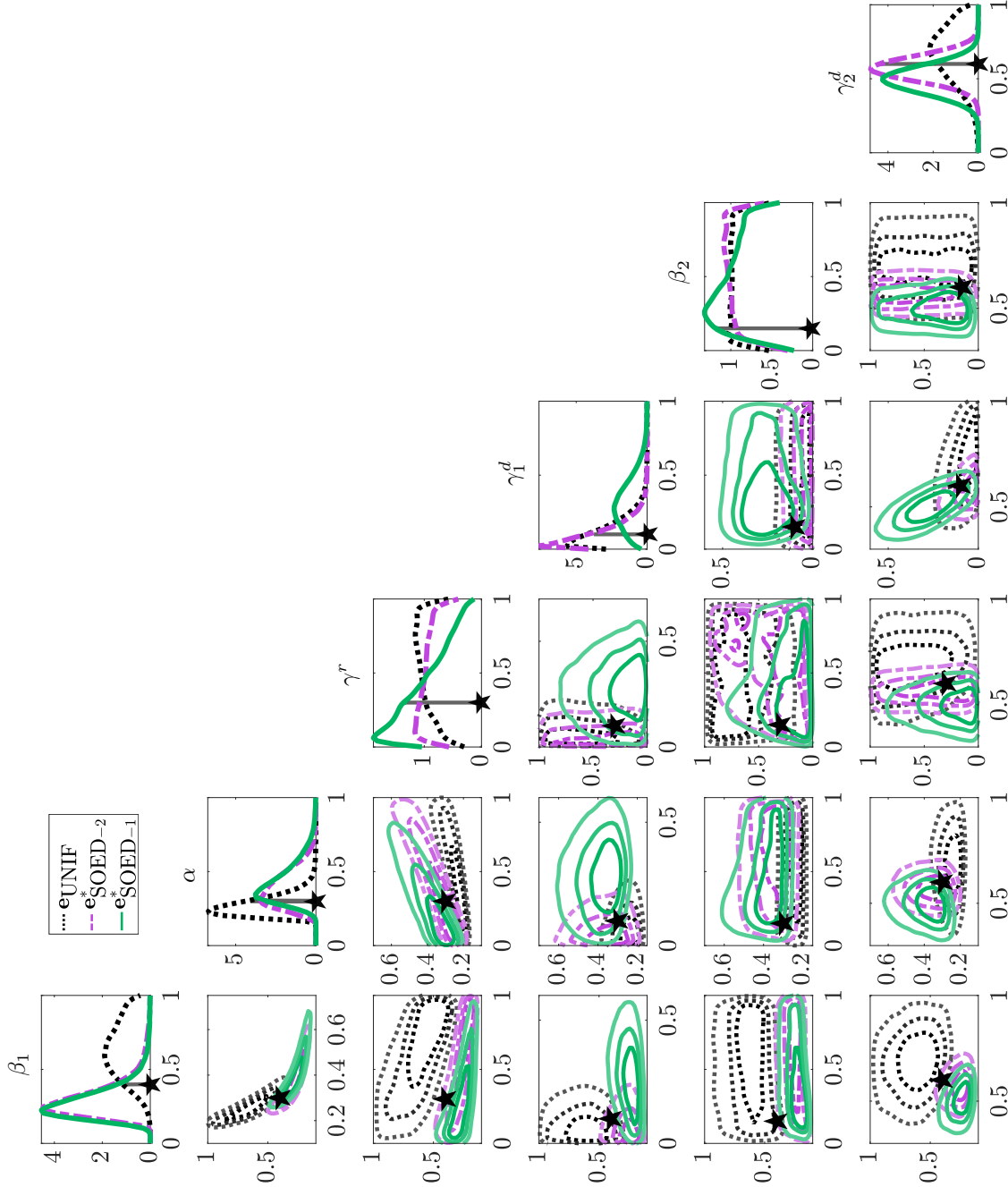


FIGURE 5.2. Visualization of the marginals of the posterior densities obtained using different observation times for the SEIR model problem in Section 5.1. The posterior depicted using the black dotted line is obtained using the uniform observation times  $e_{\text{UNIF}} = [1, 1.5, 2.0, 2.5]$ . The purple dashed line is used to visualize the posterior obtained using the two-at-a-time greedy sequential designs  $e_{\text{SOED-2}}^*$  and the solid green line corresponds to the posterior obtained using the one-at-a-time sequential optimal times  $e_{\text{SOED-1}}^*$ . In all cases, the data was synthesized using  $m_{\text{true}} = [0.4, 0.3, 0.3, 0.1, 0.15, 0.6]^T$ , visualized with a black star and perturbed by noise.

divergence, we have:

$$\begin{aligned} \mathcal{D}_{\text{KL}}(\pi_{\mathbf{m}}|_{\mathbf{e}_{\text{UNIF}}, \mathbf{d}_{\text{UNIF}}} \parallel \pi_{\mathbf{m}}) &\approx 5.1, \\ \mathcal{D}_{\text{KL}}(\pi_{\mathbf{m}}|_{\mathbf{e}_{\text{SOED-1}}^*, \mathbf{d}_{\text{SOED-1}}} \parallel \pi_{\mathbf{m}}) &\approx 6.3, \\ \text{and } \mathcal{D}_{\text{KL}}(\pi_{\mathbf{m}}|_{\mathbf{e}_{\text{SOED-2}}^*, \mathbf{d}_{\text{SOED-2}}} \parallel \pi_{\mathbf{m}}) &\approx 6.8. \end{aligned}$$

While the simultaneous planning of two experiments at a time in the greedy SOED procedure requires more solves of the SEIR system, it leads to a much better estimate of the initial rate of mortality ( $\gamma_1^d$ ) and a slightly better estimate of the final rate of mortality ( $\gamma_2^d$ ), in alignment with the slightly larger value of the KL divergence.

**Remark 5.1** (On the lack of information about the final rate of exposure  $\beta_2$ ). *We note that all the designs struggle with learning the final rate of exposure  $\beta_2$ , but this is a consequence of the transition time lying quite late in the simulation interval. Once the policies are implemented, almost all susceptible individuals are already exposed, hence the difficulty. We have also performed this experiment with a smaller value of  $\tau$ , in which case  $\beta_2$  is more accurately estimated at the expense of the precision of some of the initial rates, e. g., the initial mortality rate  $\gamma_d$ .*

In Figure 5.3, we compare the performance of the optimal designs, randomly chosen designs, and  $\mathbf{e}_{\text{UNIF}}$ . For this comparison, we extended the observation times to include two additional intervals. The optimal observation times outperform the as-soon-as-possible uniform observation times and the randomly chosen designs, and the gap greatly increases after the first experiment, since our observation times can be better geared to  $\mathbf{m}_{\text{true}}$  due to the feedback loop. It slowly tapers off after four experiments once information begins to saturate. Interestingly,  $\mathbf{e}_{\text{UNIF}}$  starts off as the worst design choice but after 6 experiments performs almost as well as the one-at-a-time greedy sequential design  $\mathbf{e}_{\text{SOED-1}}^*$ .

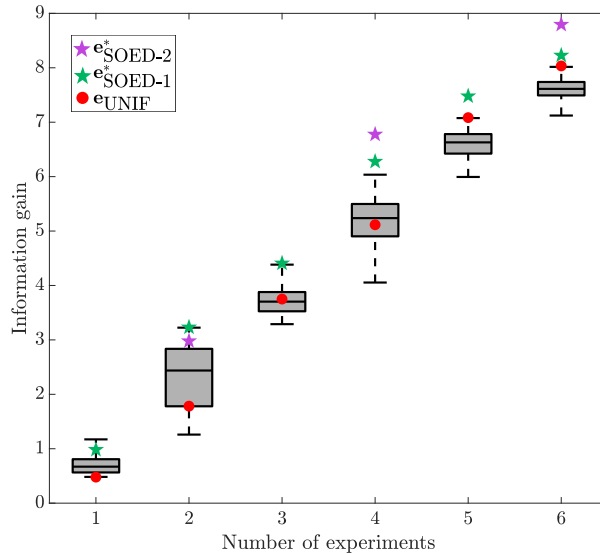


FIGURE 5.3. Boxplot comparing the effectiveness of the optimal observation times obtained for the SEIR example defined in Section 5.1 using the two-at-a-time and one-at-a-time procedures described in Section 5.1 (visualized using purple and green stars, resp.), randomly chosen observation times (visualized in black), and the uniform design  $\mathbf{e}_{\text{UNIF}}$  (red circles). To obtain the results, data was synthesized using  $\mathbf{m}_{\text{true}}$  for the optimal designs ( $\mathbf{e}_{\text{SOED-1}}^*$  and  $\mathbf{e}_{\text{SOED-2}}^*$ ) and for 100 randomly chosen observation times. For each set of data and design, the information gain or  $\mathcal{D}_{\text{KL}}(\pi_{\mathbf{m}}|_{\mathbf{e}, \mathbf{d}} \parallel \pi_{\mathbf{m}})$  was approximated using 100 000 samples from a DIRT approximation to the posterior density  $\pi_{\mathbf{m}}|_{\mathbf{e}, \mathbf{d}}$ .

**5.2. Optimal Dirichlet Data for Permeability Field Inversion.** For the second example we consider the elliptic PDE

$$(5.2) \quad -\operatorname{div}(\kappa \nabla u) = 0 \quad \text{on } \Omega = (0, 1)^2,$$

which is often used in groundwater modeling. In this example, the inverse problem consists of estimating the spatially-dependent diffusivity field  $\kappa$ , given measurements of the pressure  $u$  at some pre-determined locations  $(x_i, y_i) \in \Omega$ . To ensure  $\kappa$  is nonnegative, we impose a Gaussian prior on the log diffusivity,  $m = \log(\kappa) \sim \mathcal{N}(0, \mathcal{C}_{\text{pr}})$ , with covariance operator  $\mathcal{C}_{\text{pr}}$  defined using a squared-exponential kernel

$$c(x, z) = \sigma_v^2 \exp\left[\frac{-\|x - z\|^2}{2l^2}\right] \quad \text{for } x, z \in \Omega,$$

with  $\sigma_v = 1$  and  $l^2 = 0.1$ . Employing a truncated Karhunen-Loève expansion of the unknown diffusivity field yields the approximation

$$m(x, \mathbf{m}) \approx \sum_{i=1}^{n_m} m_i \sqrt{\lambda_i} \phi_i(x),$$

where  $\lambda_i$  and  $\phi_i(x)$  denote the  $i$ -th largest eigenvalue and eigenfunction of  $\mathcal{C}_{\text{pr}}$ , respectively, and the unknown coefficients  $m_i \sim \mathcal{N}(0, 1)$ . The Karhunen-Loève expansion is truncated after  $n_m = 16$  modes, resulting in an approximation that captures 99 percent of the weight of  $\mathcal{C}_{\text{pr}}$ .

In this example, we consider an intrusive design, i. e., we choose Dirichlet data to impose at the left and right boundary, which we parametrize as

$$(5.3a) \quad u(x = 0, y) = \exp\left(-\frac{1}{2\sigma_w} (y - e_1)^2\right),$$

$$(5.3b) \quad u(x = 1, y) = -\exp\left(-\frac{1}{2\sigma_w} (y - e_2)^2\right).$$

Homogeneous Neumann data is fixed at the top and bottom boundaries. Thus, the design  $\mathbf{e} = [e_1, e_2]$  enters into the parameter-to-state map directly through the boundary condition. The effect of different designs on the state can be seen in [Figure 5.4](#). After each experiment is performed with some prescribed boundary conditions,  $u$  is measured at three locations as visualized in [Figure 5.5](#).

Using [Algorithm 5](#), boundary conditions are chosen for five experiments in a sequential fashion. The log-diffusivity field used to synthesize the data in each experiment is visualized in [Figure 5.5](#). To speed up the construction of the FTT approximation to the joint density  $\pi_{\mathbf{e}, \mathbf{d}, \mathbf{m} | \mathbf{I}_k}$  in each stage, the design-dependent parameter-to-state map is replaced with a surrogate built using the discrete empirical interpolation method [16]. The surrogate is constructed using the Fast Forward and Inverse problems solver (FastFins) package [17] with 1000 solves of the full-order elliptic PDE, and has relative approximation error on the order of  $10^{-3}$ . One solve with the reduced-order model is approximately 60 times faster than one solve with the full model.

As in the disease modeling example outlined in the previous section, in each stage of the SOED procedure, the bridging densities are obtained by tempering the likelihood. For this example, we construct a sequence of greedy optimal designs using both A- and D-optimality criteria. In the case of D-optimality,  $N = 1000$  samples are used to approximate the expected information gain. To approximate the A-optimal sequential designs,  $N = 500$  Quasi-Monte Carlo samples are used for the outer expectation with respect to the evidence, and  $M = 1000$  Monte Carlo samples are used for the inner expectation. [Table 5.1](#) presents the computational cost (given in terms of the number of full PDE solves) of constructing the DIRT approximations to the joint density  $\pi_{\mathbf{e}_k, \mathbf{d}_k, \mathbf{m} | \mathbf{I}_{k-1}}$  and the posterior  $\pi_{\mathbf{m} | \mathbf{I}_k}$  in each SOED stage  $k = 1, \dots, 5$ , as well as the cost of evaluating  $\widehat{\Psi}_A^N(\mathbf{e}_k)$  and  $\widehat{\Psi}_D^N(\mathbf{e}_k)$  once for any choice of design  $\mathbf{e}_k \in \mathcal{E}_k$ . For this particular problem the A-optimal utility function exhibited smaller variations for different designs than the D-optimal one, so higher accuracy in the FTT surrogates to the joint densities was required (particularly in the later stages) to ensure the correct valleys and peaks were captured.

[Figure 5.5](#) compares the posterior mean and posterior pointwise variance from the posterior distribution  $\pi_{\mathbf{m} | \mathbf{e}_{1:5}, \mathbf{d}_{1:5}}$  using synthesized data from five experiments conducted with boundary conditions chosen (i) randomly and using the SOED procedure with both utility functions, (ii)  $\psi_A^k$  and (iii)  $\psi_D^k$ .

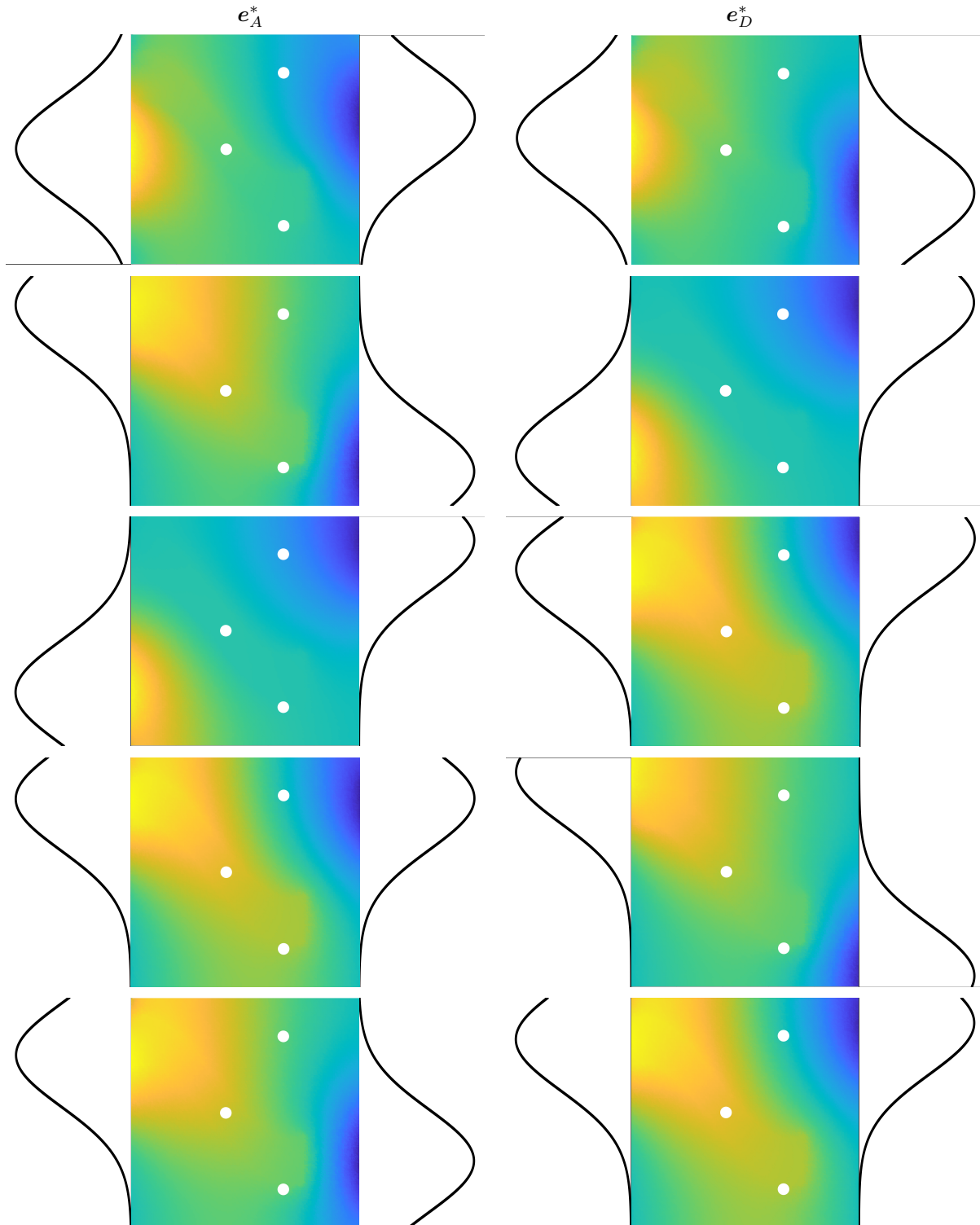


FIGURE 5.4. Visualization of optimal boundary conditions chosen using the greedy sequential procedure with the A-optimality criterion (left column) and D-optimality criterion (right column). The boundary conditions are plotted on the left and right boundaries in each figure and the corresponding state  $u$  is visualized for the true log diffusivity field.

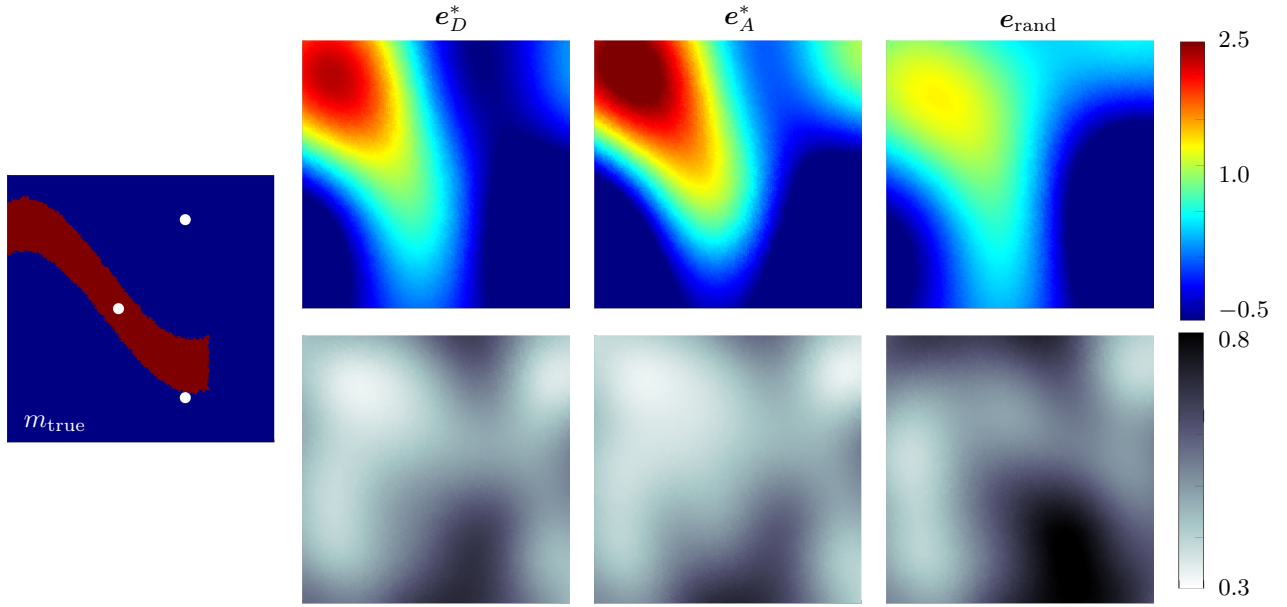


FIGURE 5.5. On the far left, the true log-diffusivity field used for synthesizing the pressure data at the three locations (visualized as white dots) is given. The top row in the  $2 \times 3$  array of images visualizes the posterior mean obtained using five experiments with boundary conditions chosen using the greedy SOED procedure with the D-optimality criterion ( $e_D^*$ ) and A-optimality criterion ( $e_A^*$ ), and a randomly chosen design ( $e_{\text{rand}}$ ). The bottom row visualizes the corresponding posterior pointwise variance for each design choice. The posterior means and variances were approximated using 100 000 samples from the corresponding approximate posterior density.

	Stage ( $k$ )	A-optimal	D-optimal
$\pi_{e_k, d_k, m   I_{k-1}}$	1	4568	4339
	2	5850	4403
	3	5403	3058
	4	4568	1747
	5	3945	1898
$\widehat{\Psi}_X^k(e_k)$	1	139	25
	2	87	24
	3	116	41
	4	139	50
	5	156	59
$\pi_{m   I_k}$	1	632	595
	2	409	518
	3	494	419
	4	632	258
	5	428	309

TABLE 5.1. Computational cost, presented in terms of the number of full-order PDE solves, for constructing the DIRT approximations to  $\pi_{e_k, d_k, m | I_{k-1}}$  and  $\pi_{m | I_k}$ , as well as the evaluation of the incremental optimality criterion  $\widehat{\Psi}_X^k$ , in each SOED stage  $k$ . Note that the A-optimality criterion  $\widehat{\Psi}_A^k$  was evaluated in parallel using 50 workers, whereas the D-optimality criterion was evaluated in serial. However, the D-optimality criterion is easily parallelizable.

As made evident by both visualizations, the optimal designs perform much better at recovering the diffusivity channel.

This observation is further strengthened in Figure 5.6, where both optimality criteria,  $\psi_A^k$  and  $\psi_D^k$ , are evaluated at the A- and D-optimal sequence of boundary conditions as well as randomly chosen boundary conditions with data synthesized using the true log-diffusivity field.

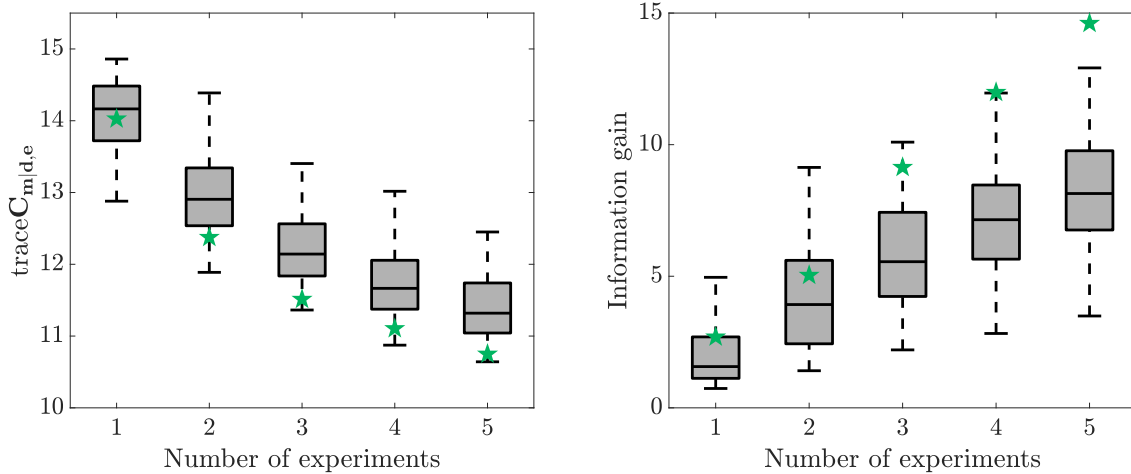


FIGURE 5.6. On the right, the information gain,  $\mathcal{D}_{\text{KL}}(\pi_{\mathbf{m}|I_k} \parallel \pi_{\mathbf{m}})$  and on the left, trace  $(\mathbf{C}_{\mathbf{m}|I_k})$ , from conducting  $k = 1, \dots, 5$  experiments. The green stars correspond to the information gained from conducting the experiments with boundary conditions chosen using the SOED procedure with the A- and D-optimality criterion. The box plot is obtained by using 100 randomly chosen boundary conditions for all five experiments. In all cases, data was synthesized using the true diffusivity field visualized in Figure 5.5.

#### ACKNOWLEDGEMENTS

The authors would like to thank Tiangang Cui and Sergey Dolgov for many helpful discussions and access to the developmental version of the DIRT MATLAB package.

#### REFERENCES

- [1] A. Alexanderian. “Optimal experimental design for infinite-dimensional Bayesian inverse problems governed by PDEs: a review”. *Inverse Problems* 37.4 (2021), p. 043001. DOI: [10.1088/1361-6420/abe10c](https://doi.org/10.1088/1361-6420/abe10c). arXiv: [2005.12998](https://arxiv.org/abs/2005.12998).
- [2] A. Alexanderian; P. J. Gloor; O. Ghattas. “On Bayesian A- and D-optimal experimental designs in infinite dimensions”. *Bayesian Analysis* 11.3 (2016). DOI: [10.1214/15-ba969](https://doi.org/10.1214/15-ba969).
- [3] A. Alexanderian; R. Nicholson; N. Petra. *Optimal design of large-scale nonlinear Bayesian inverse problems under model uncertainty*. 2022. arXiv: [2211.03952](https://arxiv.org/abs/2211.03952).
- [4] A. Alexanderian; N. Petra; G. Stadler; O. Ghattas. “A-optimal design of experiments for infinite-dimensional Bayesian linear inverse problems with regularized  $\ell_0$ -sparsification”. *SIAM Journal on Scientific Computing* 36.5 (2014), A2122–A2148. DOI: [10.1137/130933381](https://doi.org/10.1137/130933381).
- [5] A. Alexanderian; N. Petra; G. Stadler; O. Ghattas. “A fast and scalable method for A-optimal design of experiments for infinite-dimensional Bayesian nonlinear inverse problems”. *SIAM Journal on Scientific Computing* 38.1 (2016), A243–A272. DOI: [10.1137/140992564](https://doi.org/10.1137/140992564).
- [6] A. Alexanderian; N. Petra; G. Stadler; I. Sunseri. “Optimal design of large-scale Bayesian linear inverse problems under reducible model uncertainty: good to know what you don’t know”. *SIAM/ASA Journal on Uncertainty Quantification* 9.1 (2021), pp. 163–184. DOI: [10.1137/20m1347292](https://doi.org/10.1137/20m1347292). arXiv: [2006.11939](https://arxiv.org/abs/2006.11939).

- [7] A. Alexanderian; A. K. Saibaba. “Efficient D-optimal design of experiments for infinite-dimensional Bayesian linear inverse problems”. *SIAM Journal on Scientific Computing* 40.5 (2018), A2956–A2985. DOI: [10.1137/17m115712x](https://doi.org/10.1137/17m115712x).
- [8] A. C. Atkinson; A. N. Donev; R. D. Tobias. *Optimum Experimental Designs, with SAS*. Vol. 34. Oxford Statistical Science Series. Oxford: Oxford University Press, 2007.
- [9] A. Attia; A. Alexanderian; A. K. Saibaba. “Goal-oriented optimal design of experiments for large-scale Bayesian linear inverse problems”. *Inverse Problems* 34.9 (2018), p. 095009. DOI: [10.1088/1361-6420/aad210](https://doi.org/10.1088/1361-6420/aad210).
- [10] A. Attia; E. Constantinescu. “Optimal experimental design for inverse problems in the presence of observation correlations”. *SIAM Journal on Scientific Computing* 44.4 (2022), A2808–A2842. DOI: [10.1137/21m1418666](https://doi.org/10.1137/21m1418666).
- [11] A. Attia; S. Leyffer; T. S. Munson. “Stochastic learning approach for binary optimization: application to Bayesian optimal design of experiments”. *SIAM Journal on Scientific Computing* 44.2 (2022), B395–B427. DOI: [10.1137/21m1404363](https://doi.org/10.1137/21m1404363).
- [12] R. Baptista; L. Cao; J. Chen; O. Ghattas; F. Li; Y. M. Marzouk; J. T. Oden. *Bayesian model calibration for block copolymer self-assembly: likelihood-free inference and expected information gain computation via measure transport*. 2022. arXiv: [2206.11343](https://arxiv.org/abs/2206.11343).
- [13] R. Baptista; B. Hosseini; N. B. Kovachki; Y. Marzouk. *Conditional sampling with monotone GANs: from generative models to likelihood-free inference*. 2020. arXiv: [2006.06755](https://arxiv.org/abs/2006.06755).
- [14] R. Baptista; Y. Marzouk; O. Zahm. *On the representation and learning of monotone triangular transport maps*. 2020. arXiv: [2009.10303](https://arxiv.org/abs/2009.10303).
- [15] M. Brennan; D. Bigoni; O. Zahm; A. Spantini; Y. Marzouk. “Greedy inference with structure-exploiting lazy maps”. *Advances in Neural Information Processing Systems*. Ed. by H. Larochelle; M. Ranzato; R. Hadsell; M. Balcan; H. Lin. Vol. 33. NeurIPS’20. Curran Associates, Inc., 2020, pp. 8330–8342. arXiv: [1906.00031](https://arxiv.org/abs/1906.00031). URL: [https://proceedings.neurips.cc/paper\\_files/paper/2020/file/5ef20b89bab8fed38253e98a12f26316-Paper.pdf](https://proceedings.neurips.cc/paper_files/paper/2020/file/5ef20b89bab8fed38253e98a12f26316-Paper.pdf).
- [16] S. Chaturantabut; D. C. Sorensen. “Nonlinear model reduction via discrete empirical interpolation”. *SIAM Journal on Scientific Computing* 32.5 (2010), pp. 2737–2764. DOI: [10.1137/090766498](https://doi.org/10.1137/090766498).
- [17] T. Cui. *Fast Forward and Inverse problems solver (FastFInS)*. 2022. URL: <https://github.com/fastfins/fastfins.m>.
- [18] T. Cui. *Deep Inverse Rosenblatt Transport (DIRT)*. 2023. URL: <https://github.com/DeepTransport/deep-tensor>.
- [19] T. Cui; S. Dolgov. “Deep composition of tensor-trains using squared inverse Rosenblatt transports”. *Foundations of Computational Mathematics* 22.6 (2021), pp. 1863–1922. DOI: [10.1007/s10208-021-09537-5](https://doi.org/10.1007/s10208-021-09537-5).
- [20] T. Cui; S. Dolgov; O. Zahm. “Scalable conditional deep inverse Rosenblatt transports using tensor trains and gradient-based dimension reduction”. *Journal of Computational Physics* 485 (2023), p. 112103. DOI: [10.1016/j.jcp.2023.112103](https://doi.org/10.1016/j.jcp.2023.112103). arXiv: [2106.04170](https://arxiv.org/abs/2106.04170).
- [21] T. Cui; S. Dolgov; O. Zahm. *Self-reinforced polynomial approximation methods for concentrated probability densities*. 2023. arXiv: [2303.02554](https://arxiv.org/abs/2303.02554).
- [22] T. Cui; K. J. Law; Y. M. Marzouk. “Dimension-independent likelihood-informed MCMC”. *Journal of Computational Physics* 304 (2016), pp. 109–137. DOI: [10.1016/j.jcp.2015.10.008](https://doi.org/10.1016/j.jcp.2015.10.008).
- [23] T. J. Dodwell; C. Ketelsen; R. Scheichl; A. L. Teckentrup. “A hierarchical multilevel Markov Chain Monte Carlo algorithm with applications to uncertainty quantification in subsurface flow”. *SIAM/ASA Journal on Uncertainty Quantification* 3.1 (2015), pp. 1075–1108. DOI: [10.1137/130915005](https://doi.org/10.1137/130915005). arXiv: [1303.7343](https://arxiv.org/abs/1303.7343).
- [24] S. Dolgov; K. Anaya-Izquierdo; C. Fox; R. Scheichl. “Approximation and sampling of multivariate probability distributions in the tensor train decomposition”. *Statistics and Computing* 30.3 (2019), pp. 603–625. DOI: [10.1007/s11222-019-09910-z](https://doi.org/10.1007/s11222-019-09910-z). arXiv: [1810.01212](https://arxiv.org/abs/1810.01212).

- [25] A. Foster; D. R. Ivanova; I. Malik; T. Rainforth. “Deep adaptive design: amortizing sequential Bayesian experimental design”. *Proceedings of the 38th International Conference on Machine Learning*. Ed. by M. Meila; T. Zhang. Vol. 139. Proceedings of Machine Learning Research. PMLR, 2021, pp. 3384–3395. URL: <https://proceedings.mlr.press/v139/foster21a.html>.
- [26] A. Foster; M. Jankowiak; M. O’Meara; Y. W. Teh; T. Rainforth. “A unified stochastic gradient approach to designing Bayesian-optimal experiments”. *Proceedings of the 23rd International Conference on Artificial Intelligence and Statistics*. Ed. by S. Chiappa; R. Calandra. Vol. 108. Proceedings of Machine Learning Research. PMLR, 2020, pp. 2959–2969. URL: <https://proceedings.mlr.press/v108/foster20a.html>.
- [27] A. Gelman; X.-L. Meng. “Simulating normalizing constants: from importance sampling to bridge sampling to path sampling”. *Statistical Science* 13.2 (1998). DOI: [10.1214/ss/1028905934](https://doi.org/10.1214/ss/1028905934).
- [28] A. L. Gibbs; F. E. Su. “On choosing and bounding probability metrics”. *International Statistical Review* 70.3 (2002), pp. 419–435. DOI: [10.2307/1403865](https://doi.org/10.2307/1403865).
- [29] E. Haber; L. Horesh; L. Tenorio. “Numerical methods for experimental design of large-scale linear ill-posed inverse problems”. *Inverse Problems* 24.5 (2008), pp. 055012, 17. DOI: [10.1088/0266-5611/24/5/055012](https://doi.org/10.1088/0266-5611/24/5/055012).
- [30] W. K. Hastings. “Monte Carlo sampling methods using Markov chains and their applications”. *Biometrika* 57.1 (1970), pp. 97–109. DOI: [10.1093/biomet/57.1.97](https://doi.org/10.1093/biomet/57.1.97).
- [31] X. Huan. “Numerical Approaches for Sequential Bayesian Optimal Experimental Design”. PhD thesis. 2015. URL: <http://hdl.handle.net/1721.1/101442>.
- [32] X. Huan; Y. Marzouk. “Gradient-based stochastic optimization methods in Bayesian experimental design”. *International Journal for Uncertainty Quantification* 4.6 (2014), pp. 479–510. DOI: [10.1615/int.j.uncertaintyquantification.2014006730](https://doi.org/10.1615/int.j.uncertaintyquantification.2014006730).
- [33] X. Huan; Y. M. Marzouk. “Simulation-based optimal Bayesian experimental design for nonlinear systems”. *Journal of Computational Physics* 232.1 (2013), pp. 288–317. DOI: [10.1016/j.jcp.2012.08.013](https://doi.org/10.1016/j.jcp.2012.08.013).
- [34] K. Koval; A. Alexanderian; G. Stadler. “Optimal experimental design under irreducible uncertainty for linear inverse problems governed by PDEs”. *Inverse Problems* 36.7 (2020), p. 075007. DOI: [10.1088/1361-6420/ab89c5](https://doi.org/10.1088/1361-6420/ab89c5).
- [35] J. Kruse; G. Detommaso; U. Köthe; R. Scheichl. *HINT: hierarchical invertible neural transport for density estimation and Bayesian inference*. 2019. arXiv: [1905.10687](https://arxiv.org/abs/1905.10687).
- [36] D. V. Lindley. “On a measure of the information provided by an experiment”. *The Annals of Mathematical Statistics* 27.4 (1956), pp. 986–1005. DOI: [10.1214/aoms/1177728069](https://doi.org/10.1214/aoms/1177728069).
- [37] Q. Long; M. Scavino; R. Tempone; S. Wang. “Fast estimation of expected information gains for Bayesian experimental designs based on Laplace approximations”. *Computer Methods in Applied Mechanics and Engineering* 259 (2013), pp. 24–39. DOI: [10.1016/j.cma.2013.02.017](https://doi.org/10.1016/j.cma.2013.02.017).
- [38] T. A. E. Moselhy; Y. M. Marzouk. “Bayesian inference with optimal maps”. *Journal of Computational Physics* 231.23 (2012), pp. 7815–7850. DOI: [10.1016/j.jcp.2012.07.022](https://doi.org/10.1016/j.jcp.2012.07.022).
- [39] I. Neitzel; K. Pieper; B. Vexler; D. Walter. “A sparse control approach to optimal sensor placement in PDE-constrained parameter estimation problems”. *Numerische Mathematik* 143.4 (2019), pp. 943–984. DOI: [10.1007/s00211-019-01073-3](https://doi.org/10.1007/s00211-019-01073-3).
- [40] I. Oseledets; E. Tyrtshnikov. “TT-cross approximation for multidimensional arrays”. *Linear Algebra and its Applications* 432.1 (2010), pp. 70–88. DOI: [10.1016/j.laa.2009.07.024](https://doi.org/10.1016/j.laa.2009.07.024).
- [41] G. Papamakarios; E. Nalisnick; D. Jimenez Rezende; S. Mohamed; B. Lakshminarayanan. “Normalizing flows for probabilistic modeling and inference”. *Journal of Machine Learning Research* 22.57 (2021), pp. 1–64. URL: <https://www.jmlr.org/papers/v22/19-1028.html>.
- [42] M. D. Parno; Y. M. Marzouk. “Transport map accelerated Markov Chain Monte Carlo”. *SIAM/ASA Journal on Uncertainty Quantification* 6.2 (2018), pp. 645–682. DOI: [10.1137/17m1134640](https://doi.org/10.1137/17m1134640).
- [43] A. Pázman. *Foundations of Optimum Experimental Design*. Vol. 14. Mathematics and its Applications. Translated from the Czech. Springer, 1986.

- [44] F. Pukelsheim. *Optimal Design of Experiments*. Vol. 50. Classics in Applied Mathematics. Reprint of the 1993 original. Philadelphia, PA: Society for Industrial and Applied Mathematics (SIAM), 2006. DOI: [10.1137/1.9780898719109](https://doi.org/10.1137/1.9780898719109).
- [45] P. B. Rohrbach; S. Dolgov; L. Grasedyck; R. Scheichl. “Rank bounds for approximating Gaussian densities in the tensor-train format”. *SIAM/ASA Journal on Uncertainty Quantification* 10.3 (2022), pp. 1191–1224. DOI: [10.1137/20m1314653](https://doi.org/10.1137/20m1314653).
- [46] M. Rosenblatt. “Remarks on a multivariate transformation”. *The Annals of Mathematical Statistics* 23.3 (1952), pp. 470–472. DOI: [10.1214/aoms/1177729394](https://doi.org/10.1214/aoms/1177729394).
- [47] E. G. Tabak; C. V. Turner. “A family of nonparametric density estimation algorithms”. *Communications on Pure and Applied Mathematics* 66.2 (2012), pp. 145–164. DOI: [10.1002/cpa.21423](https://doi.org/10.1002/cpa.21423).
- [48] D. Uciński. *Optimal Measurement Methods for Distributed Parameter System Identification*. Systems and Control Series. Boca Raton, FL: CRC Press, 2005. DOI: [10.1201/9780203026786](https://doi.org/10.1201/9780203026786).
- [49] C. Villani. *Optimal Transport*. Vol. 338. Grundlehren der Mathematischen Wissenschaften. Springer Berlin Heidelberg, 2009. DOI: [10.1007/978-3-540-71050-9](https://doi.org/10.1007/978-3-540-71050-9).
- [50] K. Wu; T. O’Leary-Roseberry; P. Chen; O. Ghattas. *Large-scale Bayesian optimal experimental design with derivative-informed projected neural network*. 2022. arXiv: [2201.07925](https://arxiv.org/abs/2201.07925).

(K. Koval) INTERDISCIPLINARY CENTER FOR SCIENTIFIC COMPUTING, HEIDELBERG UNIVERSITY, 69120 HEIDELBERG, GERMANY

*Email address:* [karina.koval@iwr.uni-heidelberg.de](mailto:karina.koval@iwr.uni-heidelberg.de)

*URL:* <https://scoop.iwr.uni-heidelberg.de>

(R. Herzog) INTERDISCIPLINARY CENTER FOR SCIENTIFIC COMPUTING, HEIDELBERG UNIVERSITY, 69120 HEIDELBERG, GERMANY

(R. Herzog) INSTITUTE FOR MATHEMATICS, HEIDELBERG UNIVERSITY, 69120 HEIDELBERG, GERMANY

*Email address:* [roland.herzog@iwr.uni-heidelberg.de](mailto:roland.herzog@iwr.uni-heidelberg.de)

*URL:* <https://scoop.iwr.uni-heidelberg.de>

(R. Scheichl) INSTITUTE FOR MATHEMATICS, HEIDELBERG UNIVERSITY, 69120 HEIDELBERG, GERMANY

(R. Scheichl) INTERDISCIPLINARY CENTER FOR SCIENTIFIC COMPUTING, HEIDELBERG UNIVERSITY, 69120 HEIDELBERG, GERMANY

*Email address:* [robert.scheichl@uni-heidelberg.de](mailto:robert.scheichl@uni-heidelberg.de)

*URL:* <https://katana.iwr.uni-heidelberg.de/people/rob/>